A new approach to decoherence and momentum rescaling in the surface hopping algorithm

Joseph E. Subotnik[1,a)] and Neil Shenvi[2,b)]
[1]*Department of Chemistry, University of Pennsylvania, Philadelphia, Pennsylvania 19104, USA*
[2]*Department of Chemistry, Duke University, Durham, North Carolina 27708, USA*

(Received 14 July 2010; accepted 8 October 2010; published online 11 January 2011)

As originally proposed, the fewest switches surface hopping (FSSH) algorithm does not allow for decoherence between wavefunction amplitudes on different adiabatic surfaces. In this paper, we propose an inexpensive correction to standard FSSH dynamics wherein we explicitly model the decoherence of nuclear wave packets on distinct electronic surfaces. Our augmented fewest switches surface hopping approach is conceptually simple and, thus far, it has allowed us to capture several key features of the exact quantum results. Two points in particular merit attention. First, we obtain the correct branching ratios when a quantum particle passes through more than one region of nonadiabatic coupling. Second, our formalism provides a new and natural approach for rescaling nuclear momenta after a surface hop. Both of these features should become increasingly important as surface hopping schemes are applied to higher-dimensional problems. © *2011 American Institute of Physics*. [doi:10.1063/1.3506779]

I. INTRODUCTION: NONADIABATIC DYNAMICS AND THE FEWEST SWITCHES SURFACE HOPPING ALGORITHM

As has been repeatedly emphasized in the literature[1–3] there are physical situations in which the Born–Oppenheimer (or adiabatic) approximation is not valid and an understanding of nonadiabatic effects is crucial. In particular, in order to correctly describe electron transfer,[4–6] electronic excitation transfer,[7,8] or any form of electronic relaxation,[9,10] one must be able to model the coupling between nuclear motion and electronic transitions.

Various methods have been devised for treating the feedback between the classical nuclear system and the quantum mechanical electronic system. Ehrenfest dynamics is the simplest and earliest approach.[11,12] Ehrenfest dynamics allows for feedback between the quantum and classical subsystems in an essentially mean-field way; the nuclei move on the average potential energy surface of the electronic subsystem. Unfortunately, the mean-field character of Ehrenfest dynamics means that in the asymptotic limit, the forces experienced by the nuclei do not correspond to any particular adiabatic surface.

A major breakthrough came in 1990, with the introduction of fewest switches surface hopping (FSSH).[13,14] Like Ehrenfest dynamics, FSSH allows feedback between the classical and quantum subsystems. However, FSSH requires that the nuclei always propagate on a particular electronic adiabat with hops between adiabatic surfaces (hence the name "surface hopping"). The benefit of surface hopping is that the nuclei will always experience forces corresponding to real electronic states in the asymptotic limit. Surface hopping has been successfully applied to a wide variety of systems and is probably the most popular mixed quantum-classical algorithm in use today.

Since the advent of surface hopping in the early 1990s, numerous groups have attempted to fix the known shortcomings of the FSSH algorithm. In particular, it has long been known that FSSH suffers from the problem of overcoherence: because the electronic wavefunction is propagated exactly along a particular nuclear trajectory, components of the electronic wavefunction propagating on multiple electronic surfaces will always remain coherent. This can lead to spurious results for long-time dynamics, especially if nuclei visit more than one distinct region of derivative coupling.[15] In contrast, exact quantum calculations show that wave packets propagating on multiple electronic surfaces should decohere; that is, the wave packets should separate and eventually move independently.

There exist numerous approaches in the literature for overcoming this "decoherence problem" while retaining a simple trajectory-based algorithm. First, there exist algorithms which start from the quantum Liouville equation (QLE) and derive equations of motion that yield trajectories for the full nuclear-electronic density matrix.[16–27] Second, the Meyer–Miller–Stock–Thoss[12,28,29] formalism overcomes the decoherence problem by showing that, if standard Ehrenfest trajectories are added together fully coherently (with phase), the decoherence problem vanishes by phase interference. Notably, the QLE and MMST approaches are both rigorous nonadiabatic algorithms, one based on a Taylor expansion of a partial Wigner transform and the other on a semiclassical treatment of path integrals. Third, several nonrigorous techniques have been proposed for adding decoherence directly and empirically to FSSH so as to deviate only minimally from the basic structure of the original surface hopping algorithm.[15,30–45] All of these approaches can improve

a)Author to whom correspondence should be addressed. Electronic mail: subotnik@sas.upenn.edu.
b)Electronic mail: neil.shenvi@duke.edu.

the coherence properties of semiclassical dynamics, though sometimes at the cost of greater computational requirements or substantially more complicated algorithms.

In this paper, we will introduce decoherence into the surface hopping algorithm by means of a stochastic wavefunction collapse. Such an approach is not new and was indeed followed by Truhlar, Rossky, Prezhdo, Schwartz, Hammes-Schiffer, and co-workers.[15,31–35,37–44] Furthermore, the expression we derive for the decoherence rate is similar to that derived by Neria and Nitzan[46] and Schwartz *et al.*[32] What is different in our approach is the fact that we will define extra dynamical variables that will be propagated alongside the classical position and momentum of each trajectory. The decoherence rate used in our augmented fewest switches surface hopping (A-FSSH) algorithm will be related to these additional variables, which correspond roughly to the position- and momentum-space widths of the real quantum wavefunction. Furthermore, the propagation of these additional variables yields a natural formalism for momentum rescaling following a surface hop. Our approach is loosely based on the QLE formalism, and represents a small step toward connecting FSSH dynamics with the QLE formalism in Refs. 16–18.

An outline of this article is as follows. In the remainder of this section, we define our formalism and provide some necessary mathematical and algorithmic background. In Sec. A 2, we will derive the necessary theory for incorporating decoherence into the FSSH algorithm. In particular, in Sec. II A we will compute concrete equations for expanding the Quantum Liouville Equation around a surface hopping FSSH trajectory. In Sec. II B, we will show that, if we make an instantaneous frozen Gaussian ansatz for the nuclear wave packets, there is a necessary decoherence correction to standard FSSH dynamics. In Sec. II C, we offer a step-by-step outline of the A-FSSH dynamics routine that allows for decoherence, with momentum rescaling in a new direction. In Sec. III, we test the A-FSSH algorithm on four model 1D problems, each having more than one region of derivative coupling;[15] applications to higher dimensions follow naturally and are in progress. In Sec. IV, we analyze the effect of decoherence in our quantum-classical dynamics, we compare A-FSSH to other nonadiabatic algorithms, and we discuss future directions for this research.

A. Nomenclature and background

Consider a Hamiltonian having nuclear (R) and electronic (r) degrees of freedom

$$\hat{\mathbf{H}} = V(\hat{r}, \mathbf{R}) + T_{\text{nuc}}(\mathbf{R}) \equiv \hat{V}(\mathbf{R}) + \mathbf{T}_{\text{nuc}} \equiv \hat{\mathbf{V}} + \mathbf{T}_{\text{nuc}}. \quad (1)$$

For simplicity of notation, all indices for electronic degrees of freedom will be subscripted Roman characters (e.g., i in Φ_i); indices for nuclear degrees of freedom will be superscripted Greek characters (e.g., α in R^α). Nuclear vectors will be denoted with $\vec{arrow}$ notation, and nuclear operators will be written in bold style; a hat denotes an electronic operator. This notation is nearly consistent with the notation in Refs. 47 and 48. We denote by m the mass of an electron and M the mass of a nucleus.

The adiabatic basis functions for the electronic degrees of freedom are defined by

$$\hat{V}(\vec{R})\Phi_i(r;\vec{R}) = E_i(\vec{R})\Phi_i(r;\vec{R}), \quad (2)$$

the derivative couplings are

$$d^\alpha_{jk}(\vec{R}) \stackrel{\text{def}}{=} \left\langle \Phi_j(r;\vec{R}) \middle| \frac{\partial}{\partial R^\alpha} \Phi_k(r;\vec{R}) \right\rangle, \quad (3)$$

and the forces are

$$F^\alpha_{jk}(\vec{R}) \stackrel{\text{def}}{=} -\left\langle \Phi_j(r;\vec{R}) \middle| \frac{\partial \hat{V}}{\partial R^\alpha} \middle| \Phi_k(r;\vec{R}) \right\rangle. \quad (4)$$

The Hessian, or second derivative of V, will be denoted $K^{\alpha\beta}_{ij}(\vec{R})$. Henceforward, we will restrict ourselves to the case of two adiabatic surfaces, although our results should be extendible.

Consider now a trial electronic wavefunction of the form

$$|\Psi_{el}(t)\rangle \equiv \sum_j c_j(t)|\Phi_j(R(t))\rangle \quad (5)$$

defined in terms of adiabatic eigenstates (that in turn depend on nuclear position $\vec{R}(t)$). The corresponding electronic density matrix is

$$\sigma_{ij}(R(t)) \equiv \langle \Phi_i(R(t))|\Psi_{el}\rangle\langle\Psi_{el}|\Phi_j(R(t))\rangle = c_i c_j^*. \quad (6)$$

If we assume that the nuclei move classically, with momentum $\vec{P}(t)$, then Schrodinger's equation yields

$$\frac{d\sigma_{ij}}{dt} = -\frac{i}{\hbar}\sum_k \left(H^{el}_{ik}(\vec{R})\sigma_{kj} - \sigma_{ik}H^{el}_{kj}(\vec{R})\right) - \sum_\mu \frac{P^\mu}{M^\mu}\sum_k \left(d^\mu_{ik}(\vec{R})\sigma_{kj} - \sigma_{ik}d^\mu_{kj}(\vec{R})\right). \quad (7)$$

According to Eq. (7), if we know the position and momenta of classical nuclei, propagating electronic dynamics is simple. Instead, the difficulty lies in propagating the classical dynamics, i.e., how to incorporate feedback from the electronic degrees of freedom.

B. The FSSH algorithm and frozen Gaussian models for decoherence

In order to model the nonadiabatic dynamics of heavy nuclei and light electrons semiclassically, we will work closely with the FSSH method.[13,14] The FSSH algorithm dictates that we propagate nuclear dynamics along one adiabatic surface at a time. The instantaneous hopping rate between surfaces is the smallest rate possible such that, for a swarm of particles, the fraction of particles moving along surface k matches the instantaneous electron population σ_{kk}, which is propagated independently. A hop is allowed or forbidden depending on whether there is sufficient kinetic energy in the direction of the nonadiabatic derivative coupling to allow for energy conservation. All details of the standard FSSH algorithm are presented clearly in Refs. 13 and 14 and will be reviewed in Sec. II C.

The great successes of FSSH are (i) the ability to treat bond making and breaking events by ensuring that the nuclei propagate on the correct asymptotic potential energy

surfaces, and (*ii*) the ability to rigorously close all channels that are not energetically accessible during inelastic scattering. As discussed above, the biggest failure of FSSH is its inability to recognize when two wave packets on different adiabatic surfaces have moved apart (i.e., decohered), which can lead to erroneous behavior.[13]

A few years ago, Schwartz and co-workers implemented a new surface-hopping algorithm with decoherence events,[37,38] titled mean-field with stochastic decoherence (MF-SD), which we have found helpful. Their approach can be derived as follows. If we consider the overlap between frozen Gaussians in one dimension, g_1, g_2, with centers (R_i, P_i) and (R_j, P_j) in phase space, and widths $a_R = \hbar/a_P$, the exact overlap between these wave packets is[32,46]

$$\begin{aligned}\langle g_i|g_j\rangle = &\exp\left(\frac{-1}{4a_R^2}(R_i(t)-R_j(t))^2\right)\\ &\times\exp\left(\frac{-1}{4a_P^2}(P_i(t)-P_j(t))^2\right)\\ &\times\exp\left(\frac{i}{2\hbar}(R_i(t)-R_j(t))(P_i(t)+P_j(t))\right). \quad (8)\end{aligned}$$

See Sec. II B for more details. If we allow the centers of frozen Gaussian wave packets to move according to classical mechanics for short times (e.g., Ref. 49),

$$R_i(t) = R_i(0) + \frac{P_i(0)}{M}t, \quad (9)$$

$$P_i(t) = P_i(0) + F_i(0)t, \quad (10)$$

then the absolute value of the overlap becomes

$$\begin{aligned}|\langle g_i|g_j\rangle| = &\exp\left(\frac{-1}{2Ma_R^2}(R_i(0)-R_j(0))(P_i(0)-P_j(0))t\right)\\ &\times\exp\left(\frac{-1}{2a_P^2}(P_i(0)-P_j(0))(F_i(0)-F_j(0))t\right) \quad (11)\end{aligned}$$

$$= \exp\left(-t/\tau_{FG}\right), \quad (12)$$

$$\begin{aligned}\frac{1}{\tau_{FG}} \equiv &\frac{1}{2Ma_R^2}(R_i(0)-R_j(0))(P_i(0)-P_j(0))\\ &+\frac{1}{2a_P^2}(P_i(0)-P_j(0))(F_i(0)-F_j(0)). \quad (13)\end{aligned}$$

Schwartz and co-workers argued that one should do Ehrenfest dynamics, while always collapsing the electronic wavefunction to an adiabatic state at a rate similar in spirit to Eq. (13).[37,38] However, because the Schwartz algorithm does not allow instantaneously for different (R_i, P_i) versus (R_j, P_j)—i.e., the algorithm does not account for trajectory history when deciding whether or not to collapse—one finds $1/\tau_{\text{Schwartz}}$ is not exactly equal to $1/\tau_{FG}$ (see Ref. 51). The Schwartz algorithm also requires a width of the nuclear wave packet, a_R or a_P.[50] Recently, however, based on a heuristic argument, we proposed that one could both (*i*) estimate the position and momenta of distinct nuclear wave packets on different electronic surfaces and (*ii*) avoid calculating a wave packet width by extending Ehrenfest dynamics into phase space.[52]

In this paper, our goal is to rigorously compute a decoherence rate for the standard FSSH algorithm, and we will find Eq. (13) to be very useful.

II. AUGMENTED FSSH AND DECOHERENCE

A. Moment expansions and FSSH trajectories

In order to derive a decoherence time relevant to surface-hopping dynamics, we begin with the phase space formalism of Bowler, Todorov, Horsfield, and co-workers,[48,53–55] and expand all quantum mechanical operators in moments around a central trajectory. While the cited authors have previously expanded all operators around mean-field (Ehrenfest) trajectories, we will now show that the same approach can be used also for FSSH dynamics.

To start our derivation, suppose we are running standard FSSH dynamics and we generate trajectories in phase space labeled $(\vec{R}_{SH}(t), \vec{P}_{SH}(t))$. We assume that each trajectory should roughly capture the positions of nuclei on multiple electronic surfaces at time t and, for the moment, we ignore the details of how these trajectories $(\vec{R}_{SH}(t), \vec{P}_{SH}(t))$ are calculated. Our goal is to "correct" these trajectories so that they better match true quantum dynamics as specified by the quantum Liouville equation

$$\frac{\partial}{\partial t}\hat{\boldsymbol{\rho}} = \frac{-i}{\hbar}[\hat{\mathbf{H}}, \hat{\boldsymbol{\rho}}]. \quad (14)$$

Here, $\hat{\boldsymbol{\rho}}(t) = |\Psi(t)\rangle\langle\Psi(t)|$ is the exact (nuclear plus electronic) density matrix at time t, and as discussed above, bold face denotes a nuclear matrix and a $\hat{hat}$ denotes an electronic matrix. By insisting that $(\vec{R}_{SH}(t), \vec{P}_{SH}(t))$ should be decent approximations to the centers of nuclear wave packets, computationally tractable approximations can be derived by expanding all $\hat{\boldsymbol{\rho}}, \hat{\mathbf{H}}$ in moments of $\delta\vec{\mathbf{R}} = \vec{\mathbf{R}} - \vec{R}_{SH}(t)$ and $\delta\vec{\mathbf{P}} = \vec{\mathbf{P}} - \vec{P}_{SH}(t)$.

In particular, consider the reduced electronic operators

$$\hat{\sigma}(t) = \text{Tr}_N\left(\hat{\boldsymbol{\rho}}(t)\right), \quad (15)$$

$$\delta\hat{R}^\alpha(t) = \text{Tr}_N\left(\delta\mathbf{R}^\alpha\ \hat{\boldsymbol{\rho}}(t)\right) = \text{Tr}_N\left(\left(\mathbf{R}^\alpha(t) - R^\alpha_{SH}(t)\right)\hat{\boldsymbol{\rho}}(t)\right), \quad (16)$$

$$\delta\hat{P}^\alpha(t) = \text{Tr}_N\left(\delta\mathbf{P}^\alpha\ \hat{\boldsymbol{\rho}}(t)\right) = \text{Tr}_N\left(\left(\mathbf{P}^\alpha(t) - P^\alpha_{SH}(t)\right)\hat{\boldsymbol{\rho}}(t)\right). \quad (17)$$

If we are willing to ignore second- and higher-order terms $\delta\hat{R}$ and $\delta\hat{P}$, we can find closed expressions for the equations of motion of these variables.[48,53–55]

1. An exactly diabatic representation

To see how we can obtain these quantities in practice, let us focus on the reduced density matrix $\hat{\sigma}$ in an exactly diabatic electronic basis $(|\Xi_i\rangle)$. Because our approximation is first order in the terms $\delta\hat{R}$ and $\delta\hat{P}$, we will throw out all

symmetrized moments which are second order or higher (i.e., $(\delta\hat{R})^2$, $(\delta\hat{R})^2$, $(\delta\hat{R}\delta\hat{P}+\delta\hat{P}\delta\hat{R})$). According to the definition in Eq. (15),

$$\sigma_{jk}(t) \equiv \langle \Xi_j | \mathrm{Tr}_N\left(\hat{\boldsymbol{\rho}}(t)\right) | \Xi_k \rangle = \int dR' \, \langle \Xi_j R' | \hat{\boldsymbol{\rho}}(t) | \, \Xi_k R' \rangle. \tag{18}$$

Applying Schrodinger's equation, we find

$$\frac{d}{dt}\sigma_{jk}(t) = -\frac{i}{\hbar}\int dR' \, \langle \Xi_j R' | [\hat{\mathbf{H}}, \hat{\boldsymbol{\rho}}] | \Xi_k R' \rangle \tag{19}$$

$$= -\frac{i}{\hbar}\int dP' \, \langle \Xi_j P' | [\mathbf{T}, \hat{\boldsymbol{\rho}}] | \Xi_k P' \rangle - \frac{i}{\hbar}\int dR' \, \langle \Xi_j R' | [\hat{\mathbf{V}}, \hat{\boldsymbol{\rho}}] | \Xi_k R' \rangle \tag{20}$$

$$= -\frac{i}{\hbar}\int dR' \, \langle \Xi_j R' | [\hat{\mathbf{V}}, \hat{\boldsymbol{\rho}}] | \Xi_k R' \rangle. \tag{21}$$

Expanding the potential around $\vec{R}_{SH}(t)$

$$\hat{\mathbf{V}} = \hat{V}(\vec{R}_{SH}) - \sum_\alpha \hat{F}^\alpha(\vec{R}_{SH})\delta\mathbf{R}^\alpha + \sum_{\alpha,\beta}\hat{K}^{\alpha\beta}(\vec{R}_{SH})\delta\mathbf{R}^\alpha\delta\mathbf{R}^\beta + \cdots, \tag{22}$$

and, for brevity, writing $\hat{V} \equiv \hat{V}(\vec{R}_{SH}(t))$, $\hat{F} \equiv \hat{F}(\vec{R}_{SH}(t))$, we find

$$\frac{d}{dt}\sigma_{jk}(t) = -\frac{i}{\hbar}[\hat{V}, \hat{\sigma}]_{jk} + \sum_\alpha \frac{i}{\hbar}[\hat{F}^\alpha, \delta\hat{R}^\alpha]_{jk} + \cdots. \tag{23}$$

Similar equations of motion for $\delta\hat{R}$ and $\delta\hat{P}$ are also derived in the Appendix. We report the results here:

$$\frac{d}{dt}\delta R^\alpha_{jk} = \frac{-i}{\hbar}[\hat{V}, \delta\hat{R}^\alpha]_{jk} + \frac{\delta P^\alpha_{jk}}{M^\alpha} + \cdots, \tag{24}$$

$$\delta\hat{F}^\alpha = \hat{F}^\alpha - F^\alpha_{SH}(t), \tag{25}$$

$$\frac{d}{dt}\delta P^\alpha_{jk} = \frac{-i}{\hbar}[\hat{V}, \delta\hat{P}^\alpha]_{jk} + \frac{1}{2}(\delta\hat{F}^\alpha\hat{\sigma} + \hat{\sigma}\delta\hat{F}^\alpha)_{jk} - \sum_\beta \frac{1}{2}(\hat{K}^{\alpha\beta}\delta\hat{R}^\beta + \delta\hat{R}^\beta\hat{K}^{\alpha\beta})_{jk} + \cdots. \tag{26}$$

Equations (23)–(26) were derived previously by Horsfield *et al.* in Ref. 48 for the case of Ehrenfest dynamics. We emphasize, however, that these same expansions work equally well for any other choice of a classical trajectory about which we expand, in particular the FSSH trajectories treated here.

2. An adiabatic representation

Before concluding this subsection, we note that Eqs. (23)–(26) can easily be extended from a diabatic to an adiabatic electronic basis. In this case, one recognizes that the adiabatic electronic states will depend on nuclear position and one substitutes $|\Xi_i\rangle \rightarrow |\Phi_i(R_{SH}(t)\rangle$. Thus, in this basis, our definition of σ is

$$\sigma_{jk}(t) \equiv \langle \Phi_j(\vec{R}_{SH}(t))|\mathrm{Tr}_N(\hat{\boldsymbol{\rho}}(t))|\Phi_k(\vec{R}_{SH}(t))\rangle \tag{27}$$

and the corresponding equation of motion has one extra term coming from the time dependence of $\vec{R}_{SH}(t)$ and the spatial dependence of $|\Phi_i\rangle$ and $|\Phi_j\rangle$:

$$\frac{d}{dt}\sigma_{jk}(t) = -\frac{i}{\hbar}[\hat{V}, \hat{\sigma}]_{jk} + \sum_\alpha \frac{i}{\hbar}[\hat{F}^\alpha, \delta\hat{R}^\alpha]_{jk} - \sum_\alpha \frac{P^\alpha_{SH}}{M^\alpha}[\hat{d}^\alpha, \hat{\sigma}]_{jk} + \cdots. \tag{28}$$

Similar equations for $\delta\hat{R}$ and $\delta\hat{P}$ are

$$\frac{d}{dt}\delta R^\alpha_{jk} = \frac{-i}{\hbar}[\hat{V}, \delta\hat{R}^\alpha]_{jk} + \frac{\delta P^\alpha_{jk}}{M^\alpha} - \sum_\beta \frac{P^\beta_{SH}}{M^\beta}[\hat{d}^\beta, \delta\hat{R}^\alpha]_{jk} + \cdots, \tag{29}$$

$$\frac{d}{dt}\delta P^\alpha_{jk} = \frac{-i}{\hbar}[\hat{V}, \delta\hat{P}^\alpha]_{jk} + \frac{1}{2}(\delta\hat{F}^\alpha\hat{\sigma} + \hat{\sigma}\delta\hat{F}^\alpha)_{jk} - \sum_\beta \frac{1}{2}(\hat{K}^{\alpha\beta}\delta\hat{R}^\beta + \delta\hat{R}^\beta\hat{K}^{\alpha\beta})_{jk} - \sum_\beta \frac{P^\beta_{SH}}{M^\beta}[\hat{d}^\beta, \delta\hat{P}^\alpha]_{jk} + \cdots. \tag{30}$$

While Eq. (30) is correct to first order in $\delta\hat{R}$, $\delta\hat{P}$, unfortunately it requires the second derivative of the potential, $K^{\alpha\beta}_{ij}$, which is very expensive computationally. For this reason, we will ignore all terms with $K^{\alpha\beta}_{ij}$ in Eq. (30), resulting in

$$\frac{d}{dt}\delta P^\alpha_{jk} = \frac{-i}{\hbar}[\hat{V}, \delta\hat{P}^\alpha]_{jk} + \frac{1}{2}(\delta\hat{F}^\alpha\hat{\sigma} + \hat{\sigma}\delta\hat{F}^\alpha)_{jk} - \sum_\beta \frac{P^\beta_{SH}}{M^\beta}[\hat{d}^\beta, \delta\hat{P}^\alpha]_{jk} + \cdots. \tag{31}$$

As a practical matter, we have found that for the numerical problems in this paper, our results are effectively unchanged by making this approximation. From a mathematical point of view, in Eq. (30), the $\hat{F}\cdot\hat{\sigma}$ terms are zeroth-order corrections and appear to dominate the first-order $\hat{K}\cdot\delta\hat{R}$ terms. As such, our hope is that Eq. (31) is a reasonable substitute for Eq. (30) in the future. Note that, according to Eq. (31), $\delta\hat{P}^\alpha_{12}$ is propagated "roughly" on $\frac{1}{2}(F^\alpha_{11}+F^\alpha_{22})$, which further coincides "roughly" with the approach of Kapral and co-workers.[16–18]

B. A stable decoherence rate

According to the equations of motion for the reduced density matrix $\hat{\sigma}(t)$ in Eqs. (23) and (28), the reduced density matrix propagates forward in time in a manner very similar to the instantaneous electronic density matrix in semiclassical dynamics ($\hat{\sigma}(R(t))$ in Eq. (7)). In fact, comparing Eq. (28) with Eq. (7), we see that the two expressions agree to zeroth

order and nearly to first order. There is only one corrective first-order term, which depends on the antisymmetric product $\frac{i}{\hbar}[\hat{F}, \delta\hat{R}]$.

In order to understand the role of this corrective term, consider the simplest case, namely, when we are operating in a region of zero derivative coupling, $F_{12} = d_{12} = 0$. In this case, working in an adiabatic basis (with $\hat{V}$ diagonal), we have according to Eq. (28)

$$\frac{d}{dt}\sigma_{12}(t) = -\frac{i}{\hbar}(V_{11} - V_{22})\,\sigma_{12} + \sum_{\alpha}\frac{i}{\hbar}\left(F_{11}^{\alpha} - F_{22}^{\alpha}\right)\delta R_{12}^{\alpha}. \tag{32}$$

Based on this result, the corrective term in Eq. (32) leads to a putative decoherence of the semiclassical wavefunction via decay of $|\sigma_{12}|^2$

$$\begin{aligned}\frac{1}{\tau_d} &= -\frac{\frac{d}{dt}|\sigma_{12}(t)|}{|\sigma_{12}(t)|} \\ &= -\frac{\frac{d}{dt}|\sigma_{12}(t)|^2}{2\,|\sigma_{12}(t)|^2} \\ &= \mathrm{Im}\sum_{\alpha}\left(\frac{\left(F_{11}^{\alpha} - F_{22}^{\alpha}\right)\delta R_{12}^{\alpha}}{\hbar\sigma_{12}}\right).\end{aligned} \tag{33}$$

Although the expression in Eq. (33) is exact (in the limit of zero derivative coupling), it is not stable because of the σ_{12} in the denominator. More specifically, if σ_{12} is near zero and δR_{12} does not cancel this term exactly, we will obtain an infinite decoherence rate. Moreover, finite precision in machine algebra can also lead to noise in the relative phase between σ_{12} and δR_{12}, and thus also a potentially chaotic estimate of a decoherence rate (since we only take the imaginary part of their ratio). For these reasons, Eq. (33) is not optimal.

1. Approximation #1: Invoking a Gaussian ansatz

Beyond Eq. (33), a better expression for the decoherence rate can be found using a Gaussian approximation for the instantaneous wavefunction at time t, $|\Psi(t)\rangle$, following the work of Schwartz, Rossky, and co-workers (see Sec. I B). Mathematically, we assume that

$$\langle\vec{r}, \vec{R}|\Psi(t)\rangle \approx c_1 g_1(\vec{R})\Phi_1(\vec{r};\vec{R}) + c_2 g_2(\vec{R})\Phi_2(\vec{r};\vec{R}), \tag{34}$$

where

$$\begin{aligned}g_i(\vec{R}) &\equiv \langle\vec{R}|g_i(\vec{R}_i(t), \vec{P}_i(t))\rangle \\ &\equiv \prod_{\alpha}\left(\frac{1}{\pi a_{R^\alpha}^2}\right)^{1/4}\exp\left(\frac{-\left(R^{\alpha} - R_i^{\alpha}(t)\right)^2}{2a_{R^\alpha}^2}\right) \\ &\quad\times\exp\left(\frac{i}{\hbar}\,P_i^{\alpha}(t)\left(R^{\alpha} - R_i^{\alpha}(t)\right)\right),\end{aligned} \tag{35}$$

$$\begin{aligned}g_i(\vec{P}) &\equiv \langle\vec{P}|g_i(\vec{R}_i(t), \vec{P}_i(t))\rangle \\ &\equiv \prod_{\alpha}\left(\frac{1}{\pi a_{P^\alpha}^2}\right)^{1/4}\exp\left(\frac{-\left(P^{\alpha} - P_i^{\alpha}(t)\right)^2}{2a_{P^\alpha}^2}\right) \\ &\quad\times\exp\left(-\frac{i}{\hbar}\,P^{\alpha}R_i^{\alpha}(t)\right).\end{aligned} \tag{36}$$

Here g_1, g_2 are a set of normalized Gaussian wave packets with centers $(\vec{R}_1(t), \vec{P}_1(t))$ and $(\vec{R}_2(t), \vec{P}_2(t))$ in phase space, and widths $\vec{a}_R$ and $\vec{a}_P$. Gaussian wave packets by definition satisfy minimal uncertainty so that $a_{P^\alpha} = \hbar/a_{R^\alpha}$ and the centers of the Gaussian wave packets are chosen as:

$$R_i^{\alpha} \equiv R_{ii}^{\alpha} \equiv R_{SH}^{\alpha}(t) + \frac{\delta R_{ii}^{\alpha}}{\sigma_{ii}}, \tag{37}$$

$$P_i^{\alpha} \equiv P_{ii}^{\alpha} \equiv P_{SH}^{\alpha}(t) + \frac{\delta P_{ii}^{\alpha}}{\sigma_{ii}}. \tag{38}$$

Using Eqs. (34)–(36) and $\hat{\boldsymbol{\rho}}(t) = |\Psi(t)\rangle\langle\Psi(t)|$, we calculate

$$\delta R_{12}^{\alpha}(t) = \mathrm{Tr}_N(\langle\Phi_1|(\mathbf{R}^{\alpha} - \vec{R}_{SH}(t))\hat{\boldsymbol{\rho}}(t)|\Phi_2\rangle), \tag{39}$$

$$= \sigma_{12}\int d\vec{R}\left(g_1(\vec{R})\left(R^{\alpha} - R_{SH}^{\alpha}(t)\right)g_2^{*}(\vec{R})\right), \tag{40}$$

$$\begin{aligned}&= \sigma_{12}\cdot\left(\frac{i}{2}\frac{\left(P_1^{\alpha} - P_2^{\alpha}\right)a_{R^\alpha}^2}{\hbar}\right. \\ &\quad\left. + \frac{1}{2}\left(R_1^{\alpha} + R_2^{\alpha}\right) - R_{SH}(t)\right)\cdot S_{FC},\end{aligned} \tag{41}$$

$$\begin{aligned}S_{FC} &= \prod_{\beta}\exp\left(\frac{-1}{4a_{R^\beta}^2}\left(R_1^{\beta} - R_2^{\beta}\right)^2\right) \\ &\quad\times\exp\left(\frac{-1}{4a_{P^\beta}^2}\left(P_1^{\beta} - P_2^{\beta}\right)^2\right) \\ &\quad\times\exp\left(-\frac{i}{2\hbar}\left(R_1^{\beta} - R_2^{\beta}\right)\left(P_1^{\beta} + P_2^{\beta}\right)\right).\end{aligned} \tag{42}$$

Because $S_{FC} \approx 1$ to zeroth order in $R_1 - R_2$ and $P_1 - P_2$, and $[\frac{1}{2}(R_1^{\alpha} + R_2^{\alpha}) - R_{SH}]$ is real and first order, we find that (again, to first order)

$$\begin{aligned}\mathrm{Im}\left(\frac{\delta R_{12}^{\alpha}}{\sigma_{12}}\right) &\approx \frac{\left(P_1^{\alpha} - P_2^{\alpha}\right)a_{R^\alpha}^2}{2\hbar} \\ &= \frac{\hbar\left(P_1^{\alpha} - P_2^{\alpha}\right)}{2a_{P^\alpha}^2} \\ &= \frac{\left(P_1^{\alpha} - P_2^{\alpha}\right)a_{R^\alpha}}{2a_{P^\alpha}}\end{aligned} \tag{43}$$

and thus, if there are no derivative couplings, the decoherence rate is

$$\frac{1}{\tau_d} = \sum_{\alpha}\left(\frac{\left(F_{11}^{\alpha} - F_{22}^{\alpha}\right)\left(P_{11}^{\alpha} - P_{22}^{\alpha}\right)}{2a_{P^\alpha}^2}\right). \tag{44}$$

Note that we have derived the decoherence rate in Eq. (44) using only a moment expansion of the Liouville equation and an instantaneous ansatz for the wavefunction at time t to be a coherent sum of Gaussian wavefunctions evolving independently. We have *not* assumed that, as a function of time, our wavefunction is always the sum of frozen Gaussians

evolving according to classical mechanics. Thus, we are able to avoid entirely the question of when the second wave packet is spawned.[56–58] Naturally, the decoherence rate in Eq. (44) agrees with the frozen Gaussian rate (Eq. (13)) up to first order in the deviations $R_1 - R_2$, $P_1 - P_2$; the missing term in Eq. (13) is second order and has presumably been ignored by our moment expansion. Thus, Eq. (44) agrees with Prezhdo, Rossky, Schwartz, and co-workers, who argued that the "momentum decoherence" term in Eq. (13) dominates the total decoherence rate.[35,37,38]

2. Approximation #2: An optimal width for wave packet overlap

While Eq. (44) is appealing, it is not useful unless we have an estimate for the width of the wave packet $a_{P^\alpha} = \hbar/a_{R^\alpha}$. Rigorously, this quantity cannot be calculated or even rationalized because we seek a classical treatment of nuclei, wherein we cannot know the width of a wave packet. Moreover, there are cases when this width plays a crucial role in dynamics and must be known as a starting condition; see Sec. III D. As a general estimate, Schwartz and co-workers previously suggested using a thermal wavelength when computing a decoherence time.[37,38] We will take a different approach. We will assume that the effective wave packet width stretches to accommodate the newly emerging particles on different surfaces so that the wave packets remain maximally connected in phase space before decoherence. Translated mathematically, we maximize $|\langle g_1|g_2\rangle|$ in Eq. (8) as a function of either a_{P^α} or a_{R^α},

$$\frac{\partial}{\partial a_R^\alpha}|\langle g_1|g_2\rangle| = 0 \quad \text{or} \quad \frac{\partial}{\partial a_P^\alpha}|\langle g_1|g_2\rangle| = 0 \tag{45}$$

leading to the equivalent equalities

$$\frac{\hbar}{a_{P^\alpha}^2} = \frac{a_{R^\alpha}^2}{\hbar} = \frac{\left|R_1^\alpha - R_2^\alpha\right|}{\left|P_1^\alpha - P_2^\alpha\right|}$$
$$\iff \frac{\left|P_1^\alpha - P_2^\alpha\right|}{a_{P^\alpha}} = \frac{\left|R_1^\alpha - R_2^\alpha\right|}{a_{R^\alpha}}. \tag{46}$$

According to Eq. (46), we are guessing an effective width for a nuclear quantum wave packet when undergoing a classical simulation. Ultimately, this leads to a nearly stable expression for the decoherence rate:

$$\frac{1}{\tau_d} \approx \sum_\alpha \frac{\left(F_{11}^\alpha - F_{22}^\alpha\right)\left(R_{11}^\alpha - R_{22}^\alpha\right)}{2\hbar}\,\mathrm{sign}\left(\frac{R_{11}^\alpha - R_{22}^\alpha}{P_{11}^\alpha - P_{22}^\alpha}\right). \tag{47}$$

3. Approximation #3: A lower bound for the decoherence rate

Equation (47) is nearly stable but not completely. The last numerical deficiency with this expression is that, because our moment expansion propagates the quantities $\delta\hat{R}^\alpha, \delta\hat{P}^\alpha$, there can be numerical problems when we divide by electronic populations in Eqs. (37) and (38). This numerical issue can be overcome by realizing that, when doing FSSH for two states, we will always expect that either $R_{11}^\alpha \approx R_{SH}(t)$ or $R_{22}^\alpha \approx R_{SH}(t)$. Without loss of generality, let us assume that we are walking on surface 1 so that $R_{11}^\alpha \approx R_{SH}(t)$ and $\delta R_{11}^\alpha \approx 0$. In this case, for all α, $R_{11}^\alpha - R_{22}^\alpha \approx -\delta R_{22}^\alpha/\sigma_{22}$, and since $\sigma_{22} < 1$, we can find a lower bound on the decoherence rate by replacing σ_{22} with unity. Therefore, we find a lower bound for the decoherence rate to be

$$\frac{1}{\tau_d} \approx \sum_\alpha \left(\frac{\left(F_{11}^\alpha - F_{22}^\alpha\right)\left(\delta R_{11}^\alpha - \delta R_{22}^\alpha\right)}{2\hbar}\right) \times \mathrm{sign}\left(\frac{\delta R_{11}^\alpha - \delta R_{22}^\alpha}{\delta P_{11}^\alpha - \delta P_{22}^\alpha}\right). \tag{48}$$

For the remainder of this paper, we will apply stochastic decoherence event at the rate $1/\tau_d$ in Eq. (48) for a series of one-dimensional model problems, and we will show that it gives a major correction to standard FSSH. Later, in Sec. IV, we will also discuss how this correction corresponds roughly to the decoherence correction we applied recently to Ehrenfest dynamics.[52]

C. An augmented FSSH algorithm step-by-step

For the sake of concreteness, we now outline the algorithm discussed above for incorporating decoherence into traditional FSSH dynamics. According to this approach, the desired quantum-classical dynamics undergo stochastic events because of both hops and collapses. These two phenomena are distinct and capture different dynamic behavior. As introduced by Tully, hops account for population exchanging between wave packets located near each other in configuration space. As discussed in the previous subsection, collapsing events account for wave packets on different surfaces moving apart in phase space. A step-by-step outline of our algorithm is as follows:

(1) As in standard FSSH, initialize the mixed quantum-classical trajectory by fixing the initial classical coordinates $\vec{R}_0, \vec{P}_0$ and electronic density matrix $\hat{\sigma}_0$ at time $t = 0$. We usually assume that we begin on one adiabatic surface, hence $\hat{\sigma}_0 = \left(\begin{smallmatrix}1&0\\0&0\end{smallmatrix}\right)$ or $\left(\begin{smallmatrix}0&0\\0&1\end{smallmatrix}\right)$. Denote by a this initial adiabatic electronic state. Set $\delta\hat{R} = \delta\hat{P} = \left(\begin{smallmatrix}0&0\\0&0\end{smallmatrix}\right)$.

(2) As in standard FSSH, between time t and $t + dt$, propagate $\vec{R}$, $\vec{P}$, $\hat{\sigma}$ according to Eqs. (7), (49), and (50)

$$\frac{dR^\alpha}{dt} = \frac{P^\alpha}{M}, \tag{49}$$
$$\frac{dP^\alpha}{dt} = F_{aa}^\alpha(\vec{R}). \tag{50}$$

Unique to A-FSSH, propagate $\delta\hat{R}$ and $\delta\hat{P}$ according to Eqs. (29) and (31), respectively.

(3) As in standard FSSH, while the nuclei are being propagated along the ath adiabatic electronic surface, at each time step, we evaluate the probability to switch to the bth surface, $\gamma_{\mathrm{hop}}^{a\to b}$. This probability is designed to match the rate at which the electronic state is changing, and it can easily be shown[13] that:

$$\gamma_{\mathrm{hop}}^{a\to b} = -\sum_\alpha \frac{2P^\alpha}{M^\alpha}\frac{\mathrm{Re}\left(d_{ba}^\alpha(\vec{R})\sigma_{ab}\right)}{\sigma_{aa}}dt. \tag{51}$$

(4) As in standard FSSH, use a random number generator to construct a random number $\zeta \in [0, 1]$.
   (a) If $\zeta > \gamma_{\text{hop}}$, do not hop. Continue to step 6.
   (b) If $\zeta < \gamma_{\text{hop}}$, there will be a hopping event if it is energetically allowed. Continue to step 5.

(5) As in standard FSSH, in order to maintain energy conservation when moving from the ath to the bth adiabatic potential energy surface, we rescale the nuclear momentum in a direction $\vec{u}_{sc}$. In standard FSSH,[13] $\vec{u}_{sc}$ is chosen to be the direction of the instantaneous nonadiabatic derivative coupling, $\vec{u}_{sc} = \vec{d}_{ab}/|\vec{d}_{ab}|$. For multidimensional problems, in contrast to traditional FSSH, we argue that one should rescale momentum in the direction $\vec{u}_{sc} = \delta\vec{P}_{bb} - \delta\vec{P}_{aa}$. See Sec. IV for discussion. If $\vec{P}_{sc}$ is the instantaneous momentum in the direction $\vec{u}_{sc}$, i.e., $\vec{P}_{sc} = (\vec{P} \cdot \vec{u}_{sc})\vec{u}_{sc}$, we require

$$\sum_{\alpha} \frac{(P^{\alpha}_{sc})^2}{2M^{\alpha}} + V_{aa}(\vec{R}) = \sum_{\alpha} \frac{\left(P^{\text{new},\alpha}_{sc}\right)^2}{2M^{\alpha}} + V_{bb}(\vec{R}). \quad (52)$$

   (a) If the upper state is not accessible, continue to step 6.
   (b) If the upper state is accessible, a hop occurs. Rescale the momentum, $\vec{P} = \vec{P}^{\text{new}}$, and translate the first moments so as to simulate a new central trajectory with $\delta R^{\alpha}_{bb} = \delta P^{\alpha}_{bb} = 0$,

$$\delta P^{\alpha}_{ij} \to \delta P^{\alpha}_{ij} - \delta_{ij}\delta P^{\alpha}_{bb}, \quad (53)$$

$$\delta R^{\alpha}_{ij} \to \delta R^{\alpha}_{ij} - \delta_{ij}\delta R^{\alpha}_{bb}. \quad (54)$$

   Now switch the labels of electronic surfaces a and b (so that we are again walking on the "ath" surface) and continue to step 6.

(6) Unique to A-FSSH, generate a second random number, $\eta \in [0, 1]$. Construct the probability for collapse to the ath adiabatic electronic state (γ_{collapse}) by evaluating

$$\gamma_{\text{collapse}} = dt \sum_{\alpha} \left[\frac{\left(F^{\alpha}_{11} - F^{\alpha}_{22}\right)\left(\delta R^{\alpha}_{11} - \delta R^{\alpha}_{22}\right)}{2\hbar} \right] \times \text{sign}\left(\frac{\delta R^{\alpha}_{11} - \delta R^{\alpha}_{22}}{\delta P^{\alpha}_{11} - \delta P^{\alpha}_{22}} \right), \quad (55)$$

   where, as above, dt is the simulation time step.
   (a) If $\eta > \gamma_{\text{collapse}}$, there is no collapsing event. Return to step 2.
   (b) If $\eta < \gamma_{\text{collapse}}$, there is a collapsing event to electronic state a. Set $\hat{\sigma} = \left(\begin{smallmatrix} 1 & 0 \\ 0 & 0 \end{smallmatrix}\right)$ or $\left(\begin{smallmatrix} 0 & 0 \\ 0 & 1 \end{smallmatrix}\right)$, depending on whether $a = 1, 2$. Set $\delta\hat{R} = \delta\hat{P} = \left(\begin{smallmatrix} 0 & 0 \\ 0 & 0 \end{smallmatrix}\right)$. Return to step 2.

III. NUMERICAL EXAMPLES

The A-FSSH algorithm described above has been tested on four model problems, the first two of which were suggested by Tully in his original FSSH paper.[13] The first problem is a dual avoided crossing and the second problem is an extended coupling problem. These problems represent good test cases because, on the one hand, the first problem requires capturing a great deal of coherence to account for Stueckelberg oscillations. On the other hand, the second problem requires capturing significant decoherence, as the wave packets on different surfaces move in totally opposite directions. For the third and fourth problems, we combine elements of problems #1 and #2, and consider two symmetric problems with regions of extended coupling. In this case, one must balance treatments of coherence versus decoherence. We find that, to a good approximation, our augmented FSSH performs well in all cases when compared with unmodified FSSH or Ehrenfest dynamics. Incidentally, in all cases we find that ignoring second derivatives and substituting Eq. (30) with Eq. (31) has a minimal effect.

All trajectory-based calculations used a time step $dt = 0.3$ a.u. for dynamic propagation. The particle started at position $x = -20$ and trajectories were stopped when the particle reached $x = \pm 25$. We ignored all trajectories that required more than 500 000 times steps, which was always less than 0.5% of the total. We sampled 2000 trajectories at each incident velocity for each model problem. Our algorithm for computing exact quantum results is described in the Appendix.

A. Dual avoided crossing

The first problem is a dual avoided crossing defined by the following diabatic curves:

$$V_{11}(x) = 0, \quad (56)$$

$$V_{22}(x) = -Ae^{-Bx^2} + E, \quad (57)$$

$$V_{12}(x) = V_{21}(x) = Ce^{-Dx^2}. \quad (58)$$

Here $A = 0.1$, $B = 0.28$, $C = 0.015$, $D = 0.06$, and $E = 0.05$. The corresponding adiabatic states are plotted in Fig. 1. Assuming that the particle comes in from the left on the lower state, it needs an initial momentum $k > 14.1$ to reach the upper state asymptotically.

Branching ratios for the different flavors of surface hopping are shown in Fig. 2. The first conclusion from these data is that, when one ignores decoherence entirely (i.e., the standard FSSH algorithm), one models the branching ratios well, with excellent agreement at high energies and moderate agreement at low energies, in agreement with Ref. 13. Next, if one adds decoherence, the results remain accurate at high energies, while at low energies, one partially corrects the erroneous large reflection coefficient found by the FSSH algorithm, moving from 14% to 8%. The exact result has less than 2% reflection. In order to further improve our calculated results, presumably we must explicitly model wave packet separation and subsequent interference, which is not possible using surface-hopping dynamics alone.

Beyond the branching ratios, we can also assess the strength of our algorithm by considering the electronic state of the outgoing particle. In Figs. 3(c) and 3(d), we plot the fictitious electronic population on the upper surface for trajectories that are transmitted or reflected on the lower surface, respectively. Although the upper channel is closed below $k = 14.1$ a.u., emerging trajectories on the lower state do have population on the upper channel according to standard FSSH.

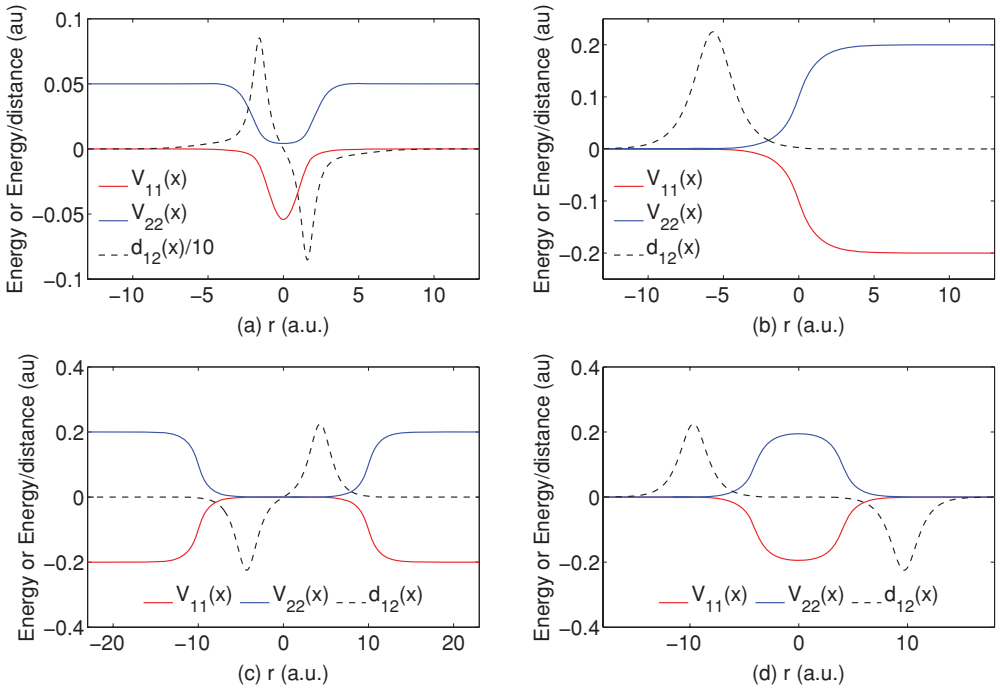

FIG. 1. The potential energy surfaces considered in this paper. The first two model problems were suggested by Tully (Ref. 13): (a) a dual avoided crossing; and (b) an extended coupling problem. The third and fourth problems are symmetrized versions of the second problem, which requires a balanced treatment of coherent versus decoherent effects: (c) a dumbbell geometry, (d) a double arch geometry.

This is a failure of the FSSH algorithm: as the wave packet emerges, the electronic state must be completely on the lower surface. Unfortunately, within the context of our A-FSSH algorithm, the fictitious population on the upper reflected channel is actually increased when we apply decoherence. Fortunately, the total probability for reflection is no larger than 8%, so this is a relatively minor effect in terms of total probabilities. Nevertheless, in order to correct this unphysical feature, one approach would be to implement free space decoherence, whereby wave packets on different surfaces with different momenta may separate even in the absence of forces. This will be discussed in Sec. IV A.

Before concluding, we mention that, according to Fig. 3(b), the number of decoherence events requested by our augmented FSSH algorithm is large at low energies but small at high energies for this dual avoided crossing. Looking at the

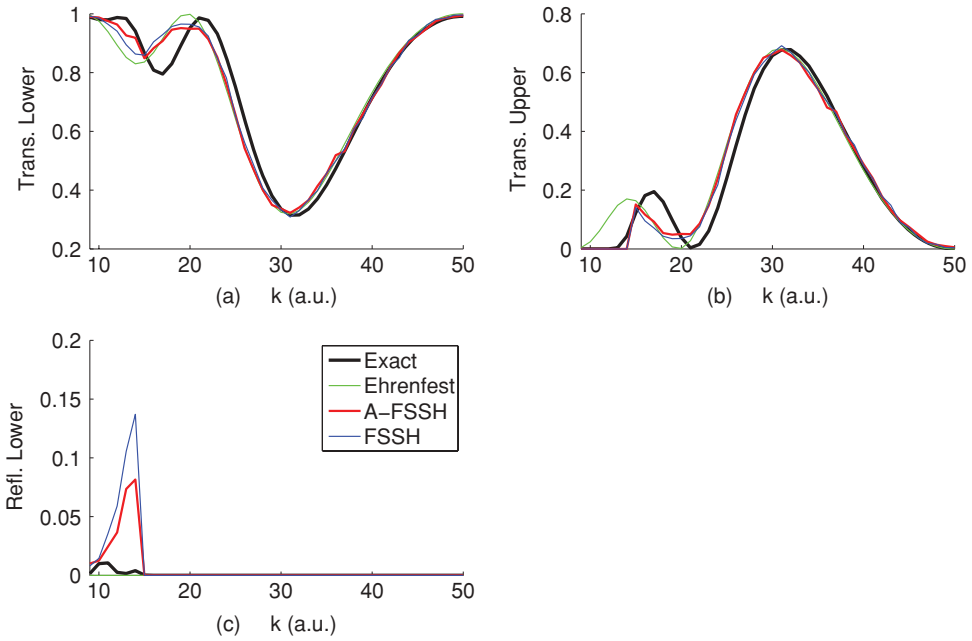

FIG. 2. Branching ratios for the first numerical model problem, a dual avoided crossing. Exact results are shown in black, Ehrenfest in green, Tully's FSSH in blue. Our A-FSSH results are shown in solid red.

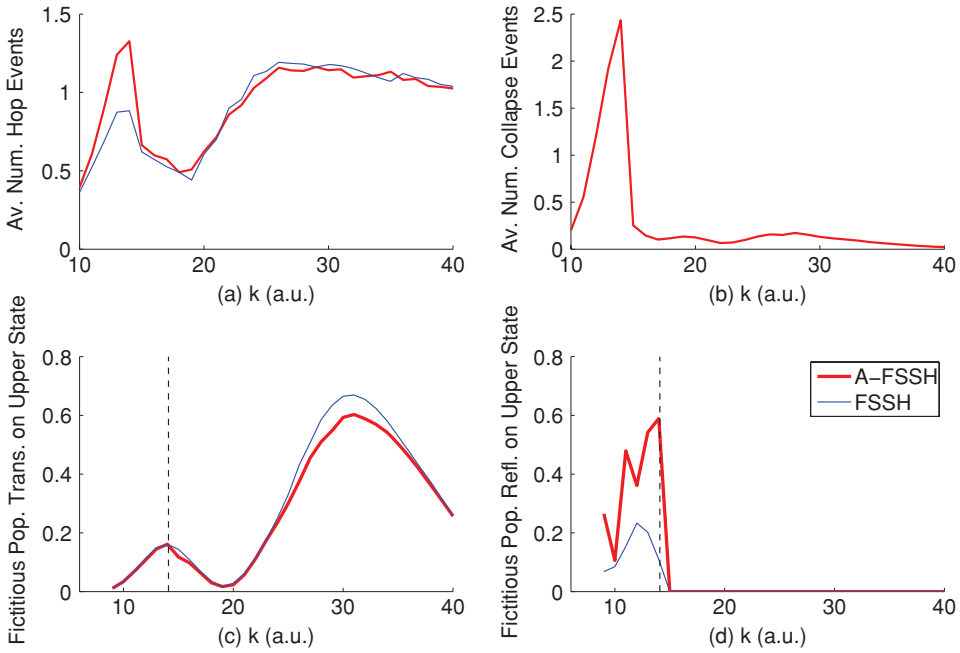

FIG. 3. (a) The average number of hopping events and (b) the average number of collapsing (or decoherence) events as a function of incoming wavevector k for the dual avoided crossing. (c) The average electronic population on the upper state for a trajectory that is transmitted on the lower state. (d) The average electronic population on the upper state for a trajectory that is reflected on the lower state. Below $k = 14.1$ a.u.—where one sees a dotted black line—the channel is closed and there should be zero population on the upper state.

branching ratios in Fig. 2, we conclude that the augmented FSSH algorithm correctly surmises when FSSH is failing and when a decoherence correction is needed. This is one encouraging development, which will be heavily exploited in the second model problem below.

B. Extended coupling

The second problem is a Hamiltonian with extended coupling defined by the following diabatic curves:

$$V_{11}(x) = A, \tag{59}$$

$$V_{22}(x) = -A, \tag{60}$$

$$V_{12}(x) = V_{21}(x) = \begin{cases} Be^{Cx} & x < 0 \\ B(2 - e^{-Cx}) & x > 0, \end{cases} \tag{61}$$

where $A = 6 \times 10^{-4}$, $B = 0.1$, and $C = 0.9$. As before, the corresponding adiabatic states are plotted in Fig. 1, and in this case, if the particle comes in from the left on the lower state, it needs an initial momentum $k > 28.2$ to reach the upper state asymptotically.

This model problem demonstrates exactly why decoherence is needed in the standard FSSH algorithm. When a particle with low kinetic energy approaches from infinity on the left, it is quickly entangled into a mixed state. As the particle reaches the origin, the derivative coupling disappears, and the wave packet on the lower surface should transmit while the wave packet on the upper surface should reflect. The essential point is that the two wave packets must separate and the interaction between them must eventually vanish. This contingency is not possible, however, according to standard FSSH, and the result is the chaotic set of reflecting branching ratios in Fig. 4. Numerically, these chaotic FSSH branching ratios are the result of a particle on the upper surface re-entering the region of derivative coupling while starting in an entangled electronic state; the initial entangled electronic density matrix responds chaotically to another region of derivative coupling. Luckily, in this case, one can average the FSSH results over k-values to find the correct and smooth branching ratios.[13] For the next model problem, however, we will show that this is not always possible.

Within the framework of FSSH, the easiest way to compute the correct branching ratios in this problem is to collapse the electronic density matrix of each particle to an adiabatic state when appropriate.[59] By doing so, we can allow the particle's wave packets to split apart, one going forward and one going backward. According to our A-FSSH algorithm, for each trajectory, we find at least one decoherence event as shown in Fig. 5(b), and as a result, we find the correct branching ratios.

Before concluding this subsection, we mention that, beyond branching ratios, according to Fig. 5(c), our augmented FSSH algorithm also predicts that:

(1) Every reflecting trajectory will carry an electronic density matrix which is entangled between the lower and upper adiabatic eigenstates.
(2) Every trajectory transmitting on the lower surface will always have less than 10% electronic population on the upper surface for $k_{\text{inc}} < 40$.

The first statement above is quite reasonable, because for reflection, the upper and lower adiabatic states are nearly isoenergetic. The second statement, however, is much

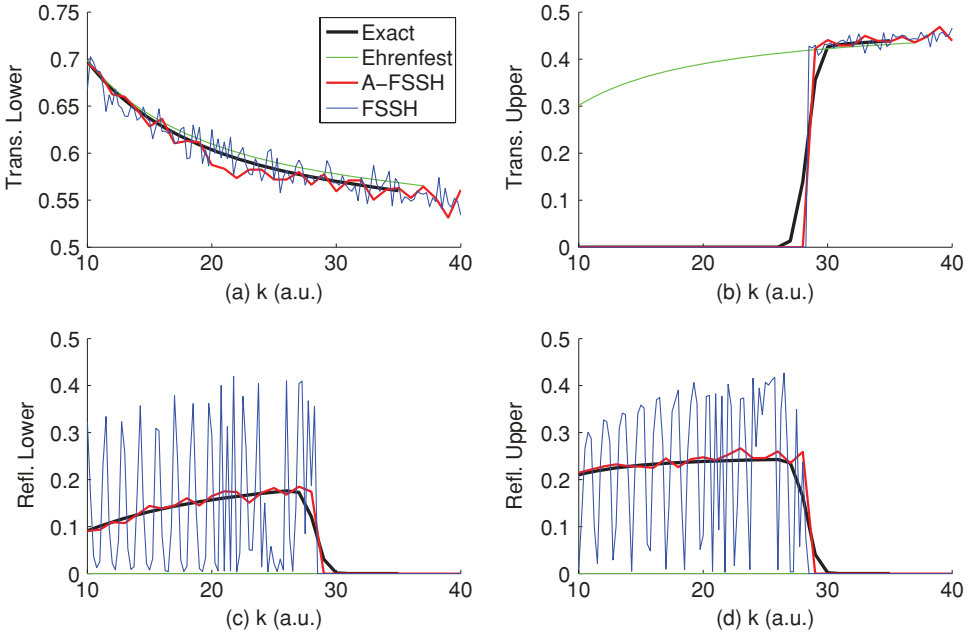

FIG. 4. The same quantities are plotted as in Fig. 2, only now for the second numerical model problem, the extended coupling Hamiltonian.

stronger, especially for high energies. On the one hand, for low energies, $k_{\text{inc}} < 28$, we find only reflection on the upper surface while transmission is possible on the lower surface. Thus, we expect to see each transmitted particle exiting the interaction region in an exact adiabatic state. On the other hand, however, at high energies $k_{\text{inc}} > 28$, the particle is transmitted on both the upper and lower surfaces. In this case, the outgoing state must be a superposition of the upper and lower electronic states at least for a short time. In a moment, however, we will demonstrate that this superposition state can be short lived and we will verify the predictions of Fig. 5(c).

C. Dumbbell geometry

The third model problem we treat is a symmetrized version of the extended coupling problem, shaped like a dumbbell. In this case, we choose the Hamiltonian to be

$$V_{11}(x) = A, \tag{62}$$

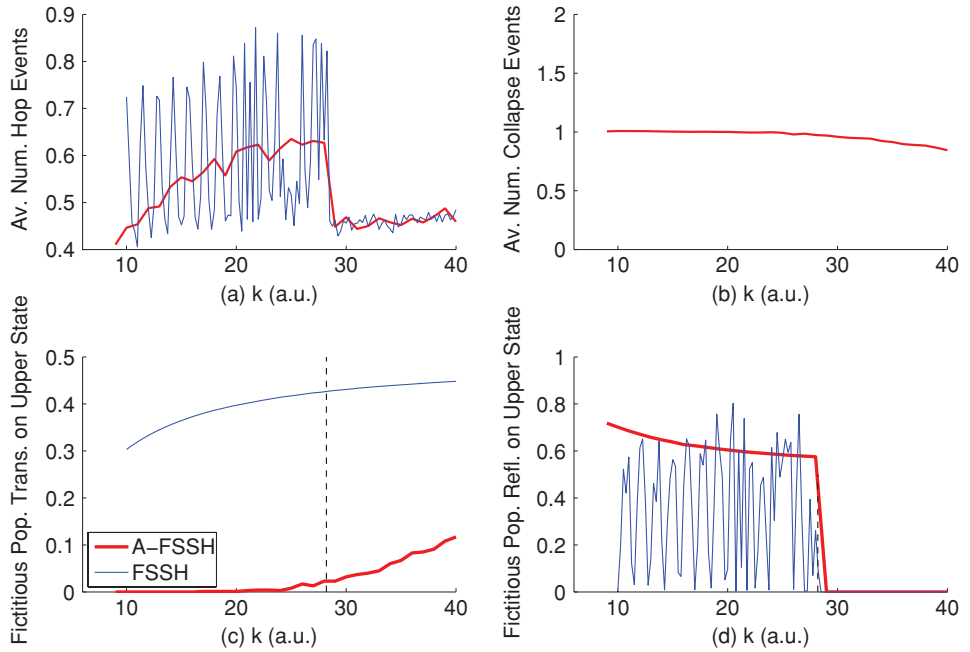

FIG. 5. The same quantities are plotted as in Fig. 3, only now for the second numerical model problem, the extended coupling Hamiltonian. In this case, the upper channel is rigorously closed below $k = 28.2$ a.u.

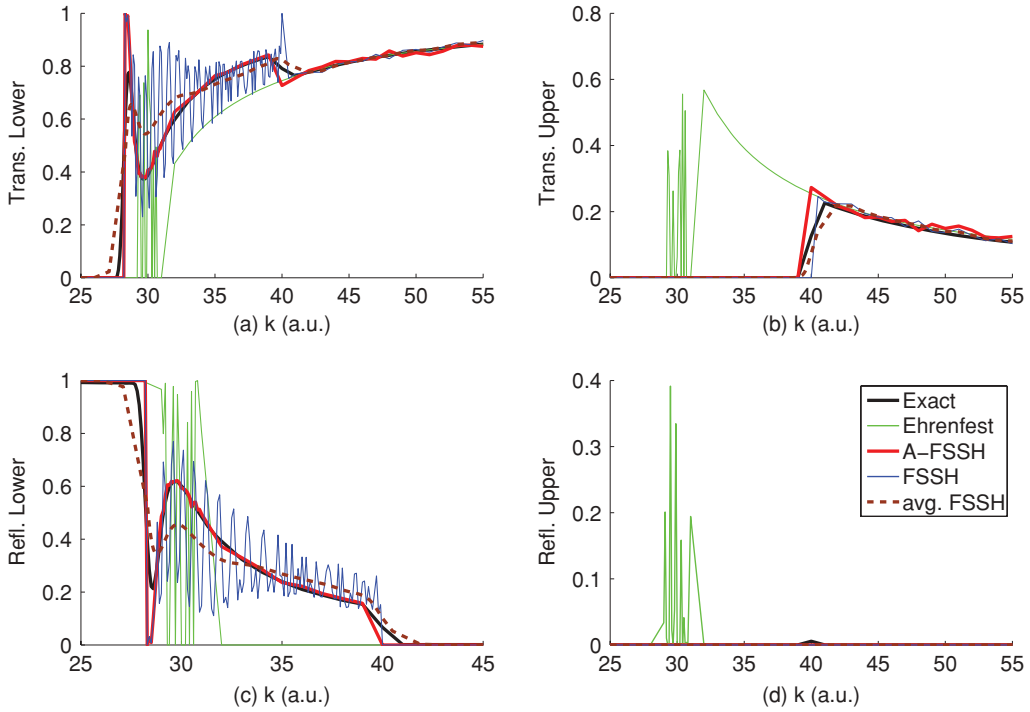

FIG. 6. The same quantities are plotted as in Fig. 2, only now for the third numerical model problem, with a dumbbell geometry. In dotted brown, we show FSSH branching ratios averaged over $a_K = k_{\rm inc}/60$ in Eq. (65). Neither the FSSH nor averaged FSSH results agree qualitatively with exact results. For the exact quantum results, the exact size of the transmission peak at $k \approx 29$ is not fully converged, and it grows proportionally to the spatial width of the incoming wave packet. According to both A-FSSH and FSSH results, we would predict there should be nearly 100% transmission in this range for a large enough spatial width. See the Appendix.

$$V_{22}(x) = -A, \tag{63}$$

$$V_{12}(x) = V_{21}(x) = \begin{cases} Be^{C(x-Z)} + B(2 - e^{C(x+Z)}) & x < -Z \\ Be^{C(x-Z)} + Be^{-C(x+Z)} & -Z < x < Z \\ B(2 - e^{-C(x-Z)}) + Be^{-C(x+Z)} & x > Z. \end{cases} \tag{64}$$

A,B,C are chosen as in model problem #2 and we set $Z = 10$. See Fig. 1 for a graphical plot of the corresponding adiabatic states and derivative coupling. As a particle comes in from the left on the lower state, it needs an initial momentum $k > 28$ or so to overcome the barrier and enter the strong coupling region in the center of the potential. Asymptotically, in order to exit on the excited channel, the particle requires an even larger momentum, $k > 40$.

The Hamiltonian in Eqs. (62)–(64) combines the difficulties of both of the previous model problems. On the one hand, we expect there will be resonance features because there are two successive regions of derivative coupling between adiabatic surfaces. So coherences between wave packets will be important. On the other hand, we also expect that for $k_{\rm inc} < 40$ the nuclear wave packet will sometimes split in two, and it will be crucial to correctly model the collapse of the electronic density matrix to the correct state (i.e., decoherence). The electronic state of a particle emerging from a region of derivative coupling is important.

In Fig. 6, we plot the branching ratios for the different outgoing channels and demonstrate the features suggested above. First, according to the exact quantum dynamical results, at momenta $k < 28$, one can tunnel between the left and right hand sides of the barrier. This feature is obviously missing from all the trajectory-based methods discussed above. At slightly higher energies, one finds a resonance peak in transmission around $k \approx 29$ onto the lower surface. Third, for $32 < k < 40$, one finds a gradual increase of transmission versus reflection (all along the lower surface). Fourth and finally, for large energies ($k > 40$), the probability of reflection vanishes and the particle is entirely transmitted either on the upper or lower surfaces.

According to Fig. 6, our augmented FSSH algorithm clearly outperforms both Ehrenfest dynamics and standard FSSH for this problem. Standard FSSH dynamics fluctuates wildly for $k < 40$. Moreover, in contrast to the previous problem, here one cannot capture the correct branching ratios by merely averaging the results over k-values. Specifically, suppose we average the FSSH branching ratios by using a Gaussian convolution to approximate the behavior of a Gaussian wave packet with momentum-space width a_K:

$$w_{\rm FSSH}^{\rm avg}(k) = \frac{1}{\sqrt{2\pi a_K^2}} \int dk' \exp\left(-\frac{(k'-k)^2}{2a_K^2(k)}\right) w_{\rm FSSH}(k'). \tag{65}$$

In dotted brown, we show that, when averaged over $a_K = k_{\rm inc}/60$, FSSH still yields qualitatively incorrect features: now, too many features are smoothed away, including the peak in transmission near $k = 29$ a.u. Here, the width $a_K = k_{\rm inc}/60$ was chosen after searching by hand for the

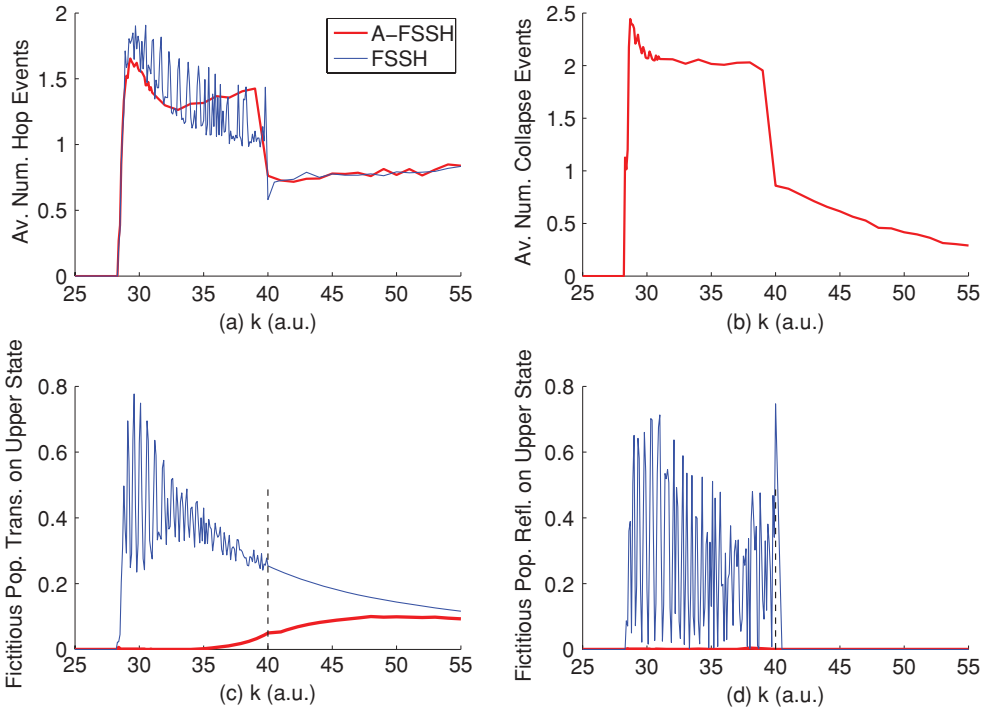

FIG. 7. The same quantities are plotted as in Fig. 3, only now for the third numerical model problem, the dumbbell geometry. In order to avoid wild oscillations in the branching ratios around $k \approx 29$ a.u., our algorithm predicts two/three decoherence events per trajectory as the particle oscillates on the upper surface. The upper surface is closed asymptotically for $k < 40$ a.u.

maximum n for which $a_K = k_{\text{inc}}/n$ smoothed away the FSSH oscillations in Fig. 6.

Encouragingly, when we introduce decoherence stochastically at the rate determined by Eq. (48), we find both smooth and accurate results. Moreover, A-FSSH captures the shape of the transmission peak (at $k \approx 29$) very well. Regarding the absolute size of that same peak, one should not rigorously compare our work to the "exact" quantum results, for the latter are somewhat sensitive to the width of the incoming wave packet (see Appendix). Finally, we mention that, like FSSH, Ehrenfest dynamics also behaves chaotically near the resonance region, and mean-field dynamics do not allow any reflection for momenta in the range $32 < k < 40$. Curiously, in this same range, the transmission ratio for FSSH dynamics appears to fluctuate between the exact results and Ehrenfest dynamics.

Regarding the state of the electronic system as the particle emerges from the scattering region, we show in Fig. 7 that for low energies there is zero population in the energetically inaccessible electronic state when we apply our decoherence correction. Furthermore, we see that in the region of resonance ($28 < k < 29$) we predict more than two decoherence events per trajectory. For these semiclassical trajectories, the particle oscillates back and forth on the upper surface before returning to the ground state, and there is a resulting peak in transmission.

D. Double arch geometry

The fourth and final model problem we treat is the converse of the third problem, where we now have one short region of extended coupling and the final adiabatic curves are shaped like a double arch. See Fig. 1 for a graphical plot of the corresponding adiabatic states and derivative couplings. The exact Hamiltonian we choose is

$$V_{11}(x) = A, \tag{66}$$

$$V_{22}(x) = -A, \tag{67}$$

$$V_{12}(x) = V_{21}(x) = \begin{cases} -Be^{C(x-Z)} + Be^{C(x+Z)} & x < -Z \\ -Be^{C(x-Z)} - Be^{-C(x+Z)} + 2B & -Z < x < Z \\ Be^{-C(x-Z)} - Be^{-C(x+Z)} & x > Z. \end{cases} \tag{68}$$

A,B,C are again chosen as in model problem #2. We choose $Z = 4$. On the lower state, there is no barrier to transmission, but for the upper state, a particle needs an initial momentum $k > 28$ to overcome the barrier. Asymptotically, in order to exit on the excited channel, there is effectively a zero energy penalty. This fourth model problem builds on model problem #2. Using the Hamiltonian in Eqs. (66)–(68) and inserting a second region of derivative coupling,[15] we now investigate what are the implications of the entangled asymptotic state described in Fig. 5.

A crucial property of this model Hamiltonian is that the branching ratios depend sensitively on the width of the incoming wave packet. First, for a wave packet that is infinitely wide in real space ($a_X = 0$ or $a_P = a_K = \infty$), i.e., a plane wave, the exact branching ratios for transmission oscillate rapidly, starting just above $k = 28$ a.u. Exact results found by time-independent scattering theory are shown in Fig. 8. These oscillations are caused by interference effects between waves

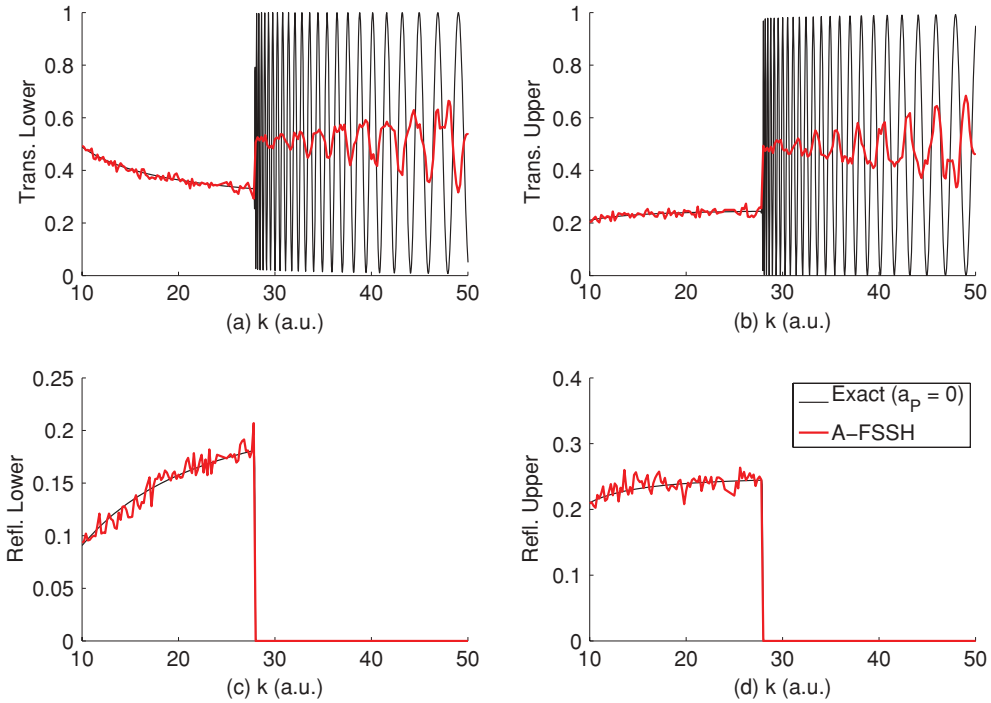

FIG. 8. A-FSSH and exact results for the fourth fourth numerical model problem, the double arch geometry. For this model problem, the exact results depend on the width of the incoming wave packet. In this figure, we present exact results from incoming wave packets with infinite spatial width ($a_X = \infty$ or $a_P = a_K = 0$, i.e. plane waves) calculated with time-independent scattering theory (Ref. 60). For these exact results, there are no oscillations below $k < 28$ a.u., while above this threshold there are full oscillations in the transmission channels. Note the decreasing frequency of these oscillations as k grows. A-FSSH agrees roughly with these exact results, in that the oscillations disappear below $k = 28$ a.u., but according to A-FSSH, these oscillations begin only slowly and grow in amplitude with k above 28 a.u. Note that these A-FSSH results correspond qualitatively to the exact results for wave packets of finite width. See Fig. 10(b).

transmitted on the upper and lower surfaces. The frequency of oscillation decreases as k_{inc} increases because, for high energies, the relative differences in velocity between the upper and lower surface become minimal.

Second, for a finite Gaussian wave packet with width a_P or a_X, the initial state is a superposition of many plane waves [as in Eq. (36)], and thus one must average plane-wave branching ratios over different P_{inc} or k_{inc} values. Mathematically, this averaging is represented precisely by Eq. (65), where a_K now represents the width of the incoming wave packet in k-space. Applying the convolution in Eq. (65), we now find that the oscillations in Fig. 8 are damped, growing only slowly in amplitude as k increases above 28 a.u. [see Fig. 10(b)]. Qualitatively, the finite wave packet results in Fig. 10(b) agree with our A-FSSH results in Fig. 8. Note the shape of the envelope function in Fig. 10(b) depends sensitively on the incoming width of the wave packet.

Having discussed Figs. 8 and 10(b) in terms of time-independent quantum mechanics, let us now turn to a time-dependent picture where we find that decoherence is crucial for understanding these figures. From a time-dependent perspective, there are actually *three* distinct energy regimes in Fig. 10(b). At low energies, $k < 28$ a.u., just as we saw in model problem #2, the wave packet launched onto the lower surface is transmitted while the wave packet on the upper surfaces reflects, so the decoherence probability is 100% for each trajectory. At medium energies, k just above 28 a.u., wave packets can be transmitted on both upper and lower surfaces. However, the wave packet on the lower surface has a much higher velocity than the wave packet on the upper surface. As such, the two wave packets partially separate before arriving at the second region of nonadiabatic derivative coupling, and we will find only partial oscillations in branching ratios. Finally, at high energies, $k \gg 28$ a.u., the size of the double arch barrier is relatively small, and the two wave packets travel effectively together in space. In this regime, we find full oscillations from 0 to 1 in the transmission branching ratios. In general, we find that the oscillations in branching ratios disappear when the wave packets separate.

The sensitivity to incoming width seen in Fig. 10(b) comes about in differentiating the medium versus high energy regime. Here, wave packet separation depends on the wave packet width, and over the flat barrier (just as in free space), spatially narrow wave packets separate more easily than spatially diffuse wave packets. From this model Hamiltonian, therefore, we conclude that sometimes decoherence rates will depend critically on the shape of the incoming wave packet and our guess for the wave packet width Eq. (46) can be impractical. More generally, for cases like these, it is unlikely that any surface-hopping algorithm can succeed quantitatively because surface-hopping algorithms seek a classical treatment of nuclei, whereby all wave packet widths are ignored implicitly.

Despite the formal difficulties above, it is comforting to see in Fig. 8 that A-FSSH yields many of the correct qualitative features of the quantum wave packet result. Namely, according to A-FSSH, there are no oscillations in branching

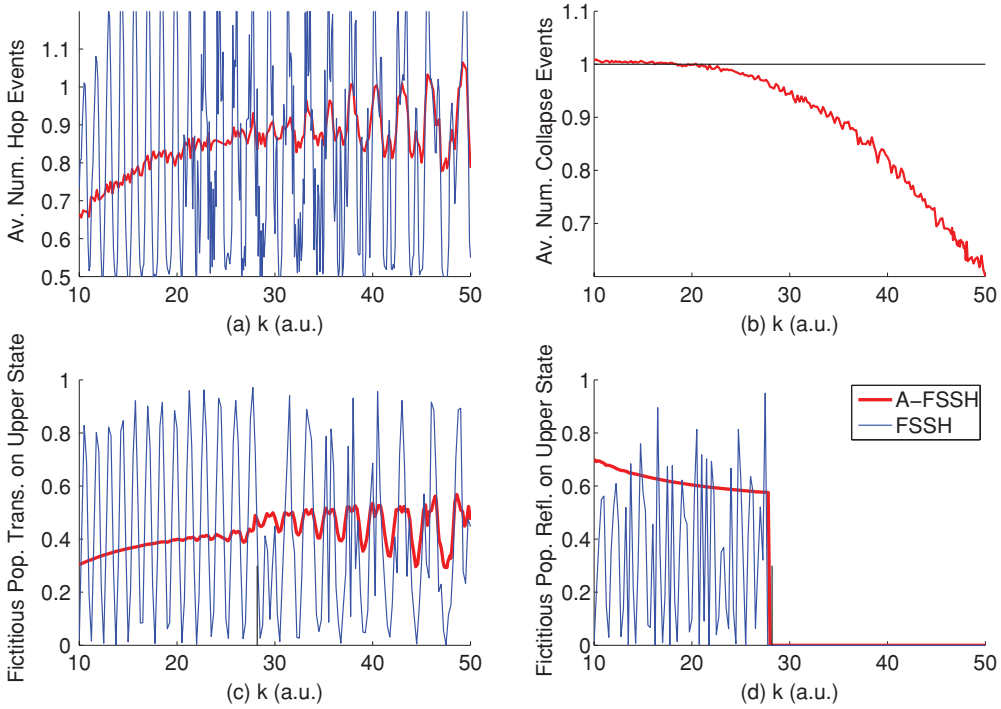

FIG. 9. The same quantities are plotted as in Fig. 3, only now for the fourth numerical model problem, the double arch geometry.

ratios at low energies, while there are oscillations that grow in amplitude as k increases beyond 28 a.u. These features are explained by Fig. 9, where we show that the number of collapsing events decreases dramatically for large k_{inc}. The A-FSSH algorithm correctly surmises when decoherence should be applied via collapsing events. In theory, one could also study A-FSSH dynamics using the incoming wave packet width instead of Eq. (46), though such information is usually not available when doing surface-hopping dynamics.

Before concluding, note that standard FSSH algorithm fails for this model problem [see Fig. 10(a)]. Of course, at low energies, FSSH predicts artificial oscillations in reflection branching ratios just as in model problem #2. More interestingly, at all energies, FSSH also predicts oscillations in transmission branching ratios. This is completely unphysical: as discussed above, the correct answer must have no oscillations in transmission at low energies and large oscillations at high energy. Because FSSH never collapses the wavefunction, however, wave packets on the different surfaces are never allowed to separate and the omnipresent oscillations in branching ratios in Fig. 8 are precisely the consequence of the fictitious electronic populations in Fig. 5(c).

IV. DISCUSSION AND CONCLUSIONS

In this article, we have presented a new algorithm for calculating a decoherence rate when performing trajectory-based FSSH dynamics. Our approach has used standard FSSH dynamics to generate one central trajectory, along which we do a moment expansion in the coupled nuclear-electron coordinates of the quantum dynamical Liouville equation. As shown by Bowler, Todorov, Horsfield, and co-workers,[48,53–55] the resulting equations of motion are solvable if we throw out all terms at second or higher order. Next, if we make an instantaneous Gaussian ansatz and assume that the wave packet stretches to accommodate relative changes in position/momentum space, as in Eq. (46), we obtain a simple decoherence rate. Finally, we have demonstrated that this rate works well for the one-dimensional model problems considered above, and that the resulting algorithm is very stable. Before concluding, we now assess the value of our dynamical routine relative to other approaches and discuss the long-term implications of this research.

A. Free space decoherence and understanding decoherence in units of $\hbar$

According to Eq. (55), wave packets separate only when they feel different forces, $F_{11} \neq F_{22}$. Thus, this equation does not allow for free space decoherence. For example, suppose that a particle enters a region of nonzero derivative coupling, and as it emerges into free space, we find $\delta R_{11} \neq \delta R_{22}$ and $\delta P_{11} \neq \delta P_{22}$. Henceforward, as the particle moves along one surface with $\hat{F} = \hat{K} = 0$, we find

$$\frac{d}{dt}\delta P_{11}^{\alpha} = 0, \quad \frac{d}{dt}\delta P_{22}^{\alpha} = 0, \tag{69}$$

$$\frac{d}{dt}\delta R_{11}^{\alpha} = \frac{\delta P_{11}^{\alpha}}{M^{\alpha}}, \quad \frac{d}{dt}\delta R_{22}^{\alpha} = \frac{\delta P_{22}^{\alpha}}{M^{\alpha}} \tag{70}$$

$$\Rightarrow \delta R_{22}^{\alpha}(t) - \delta R_{11}^{\alpha}(t) = \frac{\delta P_{22}^{\alpha}(0) - \delta P_{11}^{\alpha}(0)}{M^{\alpha}}\, t. \tag{71}$$

Thus, the particle's "images" on the different surfaces are constantly moving apart at a constant rate, and if we wait long enough, we will find $|\delta R_{11} - \delta R_{22}| \to \infty$. However, because $F_{11} = F_{22} = 0$, Eq. (55) does not demand any collapsing events for this problem.

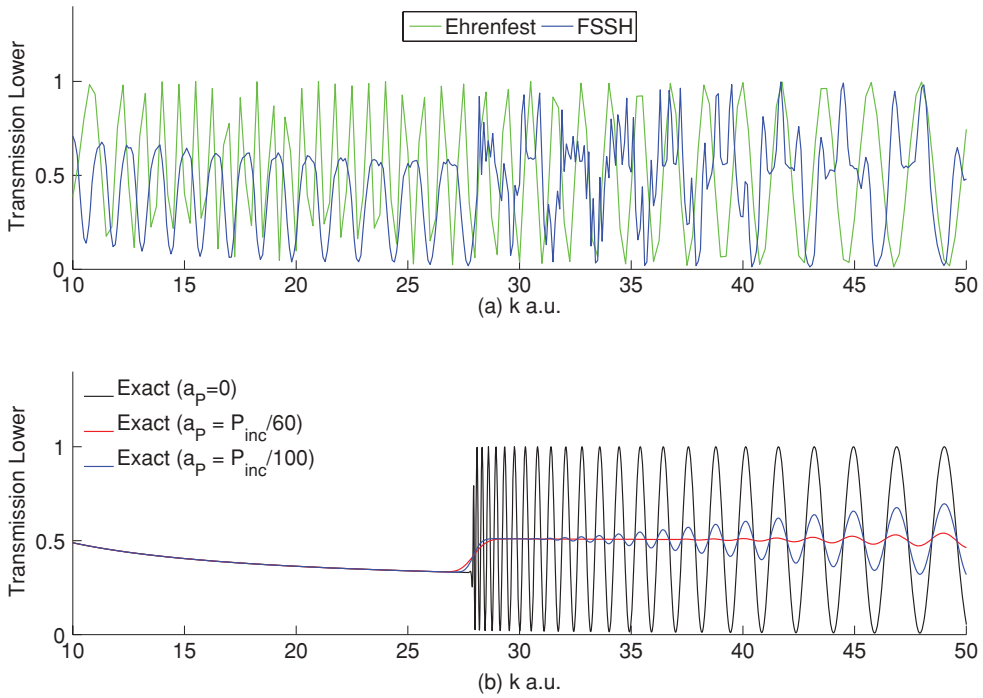

FIG. 10. The fourth model problem, the double arch geometry: (a) We plot the FSSH and Ehrenfest branching ratio for transmission along the lower surface. Both methods fail qualitatively and predict oscillations at all energies. (b) Relative to plane-wave calculations ($a_P = 0$ in black), we plot the exact branching ratios for an incoming wave packet with finite spatial width a_X and momentum width $a_P = \hbar/a_X$. These results can be obtained using either Eq. (65), or using time-dependent scattering theory. See the Appendix. According to these calculations of finite wave packets, the oscillations in transmission grow slowly in amplitude starting above $k = 28$ a.u.

From the example above, we conclude that ultimately Eq. (55) needs a correction to account for free space decoherence. In order to implement such a correction, one approach would be to incorporate the second term in Eq. (13) (which is second order in $\delta P, \delta R$) into the decoherence rate. This second-order term allows wave packets with different velocities to separate in free space, even when there is no force difference between potential energy surfaces. Using Eq. (46) to estimate a width, and again choosing a lower bound so that we can ignore factors of σ, the decoherence rate then becomes

$$\frac{1}{\tau_d} \approx \sum_\alpha \left[\frac{\left(F^\alpha_{11} - F^\alpha_{22}\right)\left(\delta R^\alpha_{11} - \delta R^\alpha_{22}\right)}{2\hbar} + \frac{\left(\delta P^\alpha_{11} - \delta P^\alpha_{22}\right)^2}{2M^\alpha \hbar} \right] \times \operatorname{sign}\left(\frac{\delta R^\alpha_{11} - \delta R^\alpha_{22}}{\delta P^\alpha_{11} - \delta P^\alpha_{22}} \right). \quad (72)$$

Interestingly, in one dimension, the second term in Eq. (72) has the appealing property of being roughly the kinetic energy of one nuclear wave packet relative to another—divided by $\hbar$. In the same spirit, the first term in Eq. (72) is roughly a difference in potential energy between two wave packets—again divided by $\hbar$. Thus, $\hbar$ emerges as the central energy scale for understanding decoherence according to our algorithm.

Equation (72) is a physically appealing decoherence rate and, in preliminary studies, it performs well on the model problems in this paper. Nevertheless, thus far, we are not convinced that the second-order term is necessary for several reasons. First, we have not rigorously derived Eq. (72) from the quantum Liouville equation. Second, suppose we were to extend the QLE expansion in Sec. II A to second order; in this case, even if we could replicate Eq. (72), there would also be other new terms. It is not clear that we should focus only on the terms arising from a frozen Gaussian ansatz. Third, empirically we have found that in Eq. (72), the second term is usually larger than the first term, which is unsatisfying. Fourth, though we cannot prove it generally, our intuition is that free-space decoherence depends more sensitively on the width of the incoming wave packet than does force-induced decoherence, which makes the former very difficult to model within surface hopping. This is certainly true for model problem #4.

Notwithstanding these reservations, decoherence expressions that account for free space [e.g., Eq. (72)] should be investigated. As a first step, new model problems are needed whereby free-space decoherence effects can be isolated that do not depend sensitively on the width of the initial nuclear wave packet (unlike model problem #4).

B. Comparison with Ehrenfest dynamics, CEID, and our previous work

Within the framework of quantum-classical methods, the simplest alternative to FSSH dynamics is mean-field (Ehrenfest) dynamics. While traditional Ehrenfest dynamics is very inexpensive, Figs. 4, 6, and 10 demonstrate this algorithm fails drastically for the model problems above. Beyond Ehrenfest dynamics, we have compared our results with the powerful correlated electron-ion dynamics (CEID) algorithm due to Bowler, Todorov, Horsfield, and co-workers.[48,53–55] CEID is a smooth nonadiabatic algorithm that computes and stores moments around Ehrenfest trajectories, and then carefully adds

together the resulting corrections to traditional Ehrenfest dynamics. Unfortunately, we have found numerical instabilities when running first-order CEID on model problem #2 above. This agrees with previous CEID work that suggests that, for large electron–phonon interactions, one must go beyond first-order CEID.[54]

Nevertheless, although first-order CEID may not be directly applicable to these problems, the stochastic approach in this paper can be easily generalized to any central trajectory of interest, and in particular Ehrenfest or mean-field dynamics. After all, we have borrowed our moment expansion in Eqs. (23)–(26) from the CEID algorithm! To fashion a stochastic algorithm based on Ehrenfest dynamics, one need only replace $(R_{SH}(t), P_{SH}(t))$ by $(R_{MF}(t), P_{MF}(t))$, which means replacing Eq. (50) with Eq. (73):

$$\frac{dP^{\alpha}}{dt} = \sum_{ab} F^{\alpha}_{ab}(\vec{R})\sigma_{ba}. \tag{73}$$

If one then runs mean-field dynamics with stochastic decoherence events at the rate of Eq. (55), one finds an algorithm somewhat similar to the Schwartz MF-SD algorithm,[37,38] and very similar in spirit[61] to our previous algorithm in Ref. 52 (provided we make the identification, $\delta R^{\alpha}_{ij}/\hbar \rightarrow$ "$\partial\sigma_{ij}/\partial P^{\alpha}$"). In the present article, however, the derivation of the decoherence rate in Eq. (55) is more rigorous than the derivation in Ref. 52; moreover, the equations of motion in Ref. 52 were only approximately correct, as they were based on Ehrenfest dynamics rather than the quantum Liouville equation.

Comparing augmented FSSH and augmented Ehrenfest dynamics, augmented FSSH has one major advantage. Namely, because FSSH obeys detailed balance approximately,[47] A-FSSH should do so as well. In particular, if we focus on the straightforward problem in Ref. 47, A-FSSH and FSSH will give identical results because $F_{11} = F_{22}$ and there is no decoherence correction according to Eq. (55). At the same time, as shown by Schmidt, Parandekar, and Tully, Ehrenfest dynamics does not obey detailed balance for this system and, according to our preliminary results, this remains true even when we allow for stochastic decoherence events around Ehrenfest trajectories.

C. Momentum rescaling and nonlocal hops/collapsing events

In the future, the most important benchmarking possible for this A-FSSH algorithm will require exploring multidimensional problems in quantum dynamics, where energy can be dissipated among many different nuclear degrees of freedom. For such problems, Tully has suggested for standard FSSH that, when a hop occurs from electronic state a to electronic state b, one should rescale the momentum in the direction of the instantaneous derivative coupling, i.e., $\vec{u}_{sc} = \vec{d}_{ab}$ in Eq. (52).[13]

The ideas presented in this paper, however, suggest a different ansatz. Here, it would appear natural that if we are going to rescale the momentum, it ought to be rescaled in the direction $\vec{u}_{sc} = \delta\vec{P}_{bb} - \delta\vec{P}_{aa}$. After all, this change in momentum space should approximate, to first order, the relative momenta of the two different wave packets in phase space. Furthermore, this solution suggests that the position coordinate as well as the momentum coordinate could be rescaled when we make a hop. The possibility of position adjustment has been explored successfully in recent years by Heller and Beck,[62] Heller *et al.*,[63] and Yang *et al.*[58] We hope to explore this idea further within the context of A-FSSH dynamics, but in practical terms, it will be difficult to achieve efficiently for on-the-fly dynamics, whereby we do not have a global functional form for each potential energy surface but must still conserve energy. Ultimately, position adjustment may be impossible unless an iterative scheme is employed which locally explores the potential energy surface whenever a hop is made.

Interestingly, for augmented Ehrenfest dynamics (with stochastic decoherence events), we have found it necessary to apply nonlocal collapsing events in order to achieve the correct branching ratios for the original Tully scattering problems.[52] In particular, we were forced to move both in real space and momentum space in order to allow a collapsing event to a forbidden electronic state. In contrast, because FSSH dynamics do not allow movement along closed channels, collapsing events in the A-FSSH algorithm can be entirely local in real space. These different treatments of forbidden states are closely tied to satisfying detailed balance.[47] Given the many possibilities raised by our approach, choosing a new direction for momentum rescaling will be addressed in a future publication.

D. Computational cost

Having demonstrated the reasons and rationale for applying decoherence to the FSSH algorithm, we want to emphasize that computational cost should *not* prevent this algorithm from being applied broadly. We first discuss electronic structure requirements. Formally, the computational cost of the algorithm proposed in Sec. A 2 is much larger than the cost of the standard FSSH algorithm. After all, according to Eq. (30), we require second derivatives (or Hessians) of the potential energy surfaces. That being said, however, if we disregard the second derivatives in Eq. (30) and instead use Eq. (31), we obtain results that are effectively identical to the exact results for the few problems considered here. Moreover, by ignoring second derivatives, the only difference in electronic structure needs between A-FSSH and FSSH dynamics is that A-FSSH requires the full gradient matrix while FSSH requires the energetic gradient along only one surface. As such, for two electronic surfaces, the A-FSSH algorithm should be only two to four times as expensive as standard FSSH. Although we have not treated the case of n electronic states in this paper, presumably the additional cost will be between n and n^2 most generally, where ideally n is a small number.

Beyond the computational cost of electronic structure calls, suppose that we were to propagate surface-hopping dynamics with two fitted potential energy surfaces. In this case, A-FSSH propagates two to four times the number of variables as FSSH, and again, A-FSSH should be only two to four times as expensive as standard FSSH.

An immediate goal for future research will be to computationally verify these statements about algorithmic scaling. If confirmed, the A-FSSH algorithm will be computationally feasible whenever standard FSSH is feasible, and our hope is that A-FSSH will be adopted and compared broadly to standard FSSH dynamics.

E. Conclusions

In conclusion, for the past twenty years, the standard FSSH algorithm has been a powerful tool for solving nonadiabatic problems in chemical dynamics without accounting for decoherence. In order to account for decoherence approximately, we have proposed an augmented algorithm that requires two modifications of the standard FSSH approach. First, in addition to the standard variables (R^α, P^α, $\hat{\sigma}$), we propagate a few more quantities that carry information about nuclear-electronic correlation ($\delta\hat{R}^\alpha$ and $\delta\hat{P}^\alpha$). Second, we allow wave packets on different surfaces to separate (i.e., decohere) by collapsing the wavefunction at the rate of Eq. (48). Soon, we will extend the algorithm here to the case of more than two electronic states. Starting with a standard FSSH code, our algorithm is easy to implement, the total computational cost should be only a factor of two or four times higher (for two electronic states), and the preliminary results are thus far very encouraging. In the future, we hope that others who are interested in nonadiabatic dynamics will implement this augmented FSSH algorithm and investigate the consequences of this new decoherence time scale.

ACKNOWLEDGMENTS

We thank Abraham Nitzan, Ryan Steele, John Tully, Bill Miller, Todd Martinez, Sharani Roy, Andrew Horsfield, David Reichman, and Mark Ratner for illuminating discussions. J.E.S. thanks the University of Pennsylvania for financial support. NS thanks the National Science Foundation (NSF-CHE-06-16849-03) and the Department of Energy under Award No. DE-SC0001011 for funding.

APPENDIX: FURTHER DETAILS

1. Equations of motion for $\delta\hat{P}$ and $\delta\hat{R}$

We now derive Eqs. (24) and (26) for $\delta\hat{R}$ and $\delta\hat{P}$ in an exactly diabatic basis. Starting with the definitions

$$\boldsymbol{\rho}^{\text{red}}_{jk}(t) \equiv \langle \Xi_j | \hat{\boldsymbol{\rho}}(t) | \Xi_k \rangle, \tag{A1}$$

$$\delta R^\alpha_{jk}(t) \equiv \langle \Xi_j | \text{Tr}_N(\delta\mathbf{R}^\alpha(t)\ \hat{\boldsymbol{\rho}}(t)) | \Xi_k \rangle, \tag{A2}$$

$$\delta P^\alpha_{jk}(t) \equiv \langle \Xi_j | \text{Tr}_N(\delta\mathbf{P}^\alpha(t)\ \hat{\boldsymbol{\rho}}(t)) | \Xi_k \rangle, \tag{A3}$$

we compute (dropping the explicit "(t)" to represent time dependence)

$$\frac{d}{dt}\delta R^\alpha_{jk} = \frac{-i}{\hbar}\langle \Xi_j | \text{Tr}_N(\delta\mathbf{R}^\alpha\ [\hat{\mathbf{H}}, \hat{\boldsymbol{\rho}}]) | \Xi_k \rangle - \frac{P^\alpha_{SH}}{M^\alpha}\sigma_{jk} \tag{A4}$$

$$= \frac{-i}{\hbar}\langle \Xi_j | \text{Tr}_N(\delta\mathbf{R}^\alpha\ [\hat{\mathbf{V}}, \hat{\boldsymbol{\rho}}]) | \Xi_k \rangle - \frac{i}{\hbar}\langle \Xi_j | \text{Tr}_N(\delta\mathbf{R}^\alpha\ [\mathbf{T}, \hat{\boldsymbol{\rho}}]) | \Xi_k \rangle - \frac{P^\alpha_{SH}}{M^\alpha}\sigma_{jk}$$

$$\approx \frac{-i}{\hbar}\langle \Xi_j | \text{Tr}_N(\delta\mathbf{R}^\alpha\ [\hat{V}(R_{SH}), \hat{\boldsymbol{\rho}}]) | \Xi_k \rangle - \frac{i}{\hbar}\text{Tr}_N\left(\delta\mathbf{R}^\alpha\ \left[\mathbf{T}, \boldsymbol{\rho}^{\text{red}}_{jk}\right]\right) - \frac{P^\alpha_{SH}}{M^\alpha}\sigma_{jk}$$

$$= \frac{-i}{\hbar}\langle \Xi_j | [\hat{V}(R_{SH}), \text{Tr}_N(\delta\mathbf{R}^\alpha\hat{\boldsymbol{\rho}})] | \Xi_k \rangle + \frac{i}{\hbar}\text{Tr}_N\left(\boldsymbol{\rho}^{\text{red}}_{jk}[\mathbf{T}, \delta\mathbf{R}^\alpha]\right) - \frac{P^\alpha_{SH}}{M^\alpha}\sigma_{jk} \tag{A5}$$

$$= \frac{-i}{\hbar}\langle \Xi_j | [\hat{V}(R_{SH}), \delta\hat{R}^\alpha] | \Xi_k \rangle + \frac{1}{M^\alpha}\text{Tr}_N\left(\boldsymbol{\rho}^{\text{red}}_{jk}\mathbf{P}^\alpha\right) - \frac{P^\alpha_{SH}}{M^\alpha}\sigma_{jk} \tag{A6}$$

$$= \frac{-i}{\hbar}[\hat{V}(R_{SH}), \delta\hat{R}^\alpha]_{jk} + \frac{\delta P^\alpha_{jk}}{M^\alpha} \tag{A7}$$

$$\frac{d}{dt}\delta P^\alpha_{jk} = \frac{-i}{\hbar}\langle \Xi_j | \text{Tr}_N(\delta\mathbf{P}^\alpha\ [\hat{\mathbf{H}}, \hat{\boldsymbol{\rho}}]) | \Xi_k \rangle - F^\alpha_{SH}(t)\sigma_{jk} \tag{A8}$$

$$= \frac{-i}{\hbar}\langle \Xi_j | \text{Tr}_N(\delta\mathbf{P}^\alpha\ [\hat{\mathbf{V}}, \hat{\boldsymbol{\rho}}]) | \Xi_k \rangle - F^\alpha_{SH}(t)\sigma_{jk} \tag{A9}$$

$$\approx \frac{-i}{\hbar}\langle \Xi_j | \text{Tr}_N(\delta\mathbf{P}^\alpha\ [\hat{V}(R_{SH}), \hat{\boldsymbol{\rho}}]) | \Xi_k \rangle + \frac{i}{\hbar}\left\langle \Xi_j \left| \text{Tr}_N\left(\delta\mathbf{P}^\alpha\left[\sum_\beta \hat{F}^\beta(R_{SH})\delta\mathbf{R}^\beta, \hat{\boldsymbol{\rho}}\right]\right)\right| \Xi_k \right\rangle \tag{A10}$$

$$- \frac{i}{2\hbar}\left\langle \Xi_j \left| \text{Tr}_N\left(\delta\mathbf{P}^\alpha\left[\sum_{\beta\gamma} \hat{K}^{\beta\gamma}\delta\mathbf{R}^\beta\delta\mathbf{R}^\gamma, \hat{\boldsymbol{\rho}}\right]\right)\right| \Xi_k \right\rangle - F^\alpha_{SH}\sigma_{jk}$$

$$\approx \frac{-i}{\hbar}[\hat{V}, \delta\hat{P}^\alpha]_{jk} + \frac{i}{\hbar}\sum_{\beta r} F^\beta_{jr}\text{Tr}_N\left(\delta\mathbf{P}^\alpha\delta\mathbf{R}^\beta\boldsymbol{\rho}^{\text{red}}_{rk}\right) - \frac{i}{\hbar}\sum_{\beta r}\text{Tr}_N\left(\delta\mathbf{P}^\alpha\boldsymbol{\rho}^{\text{red}}_{jr}\delta\mathbf{R}^\beta\right)F^\beta_{rk} - \frac{i}{2\hbar}\sum_{\beta\gamma r} K^{\beta\gamma}_{jr}\text{Tr}_N\left(\delta\mathbf{P}^\alpha\delta\mathbf{R}^\beta\delta\mathbf{R}^\gamma\boldsymbol{\rho}^{\text{red}}_{rk}\right) + \frac{i}{2\hbar}\sum_{\beta r}\text{Tr}_N\left(\delta\mathbf{P}^\alpha\boldsymbol{\rho}^{\text{red}}_{jr}\delta\mathbf{R}^\beta\delta\mathbf{R}^\gamma\right)K^{\beta\gamma}_{rk} - F^\alpha_{SH}\sigma_{jk}. \tag{A11}$$

Using the cyclic invariance of a trace and the identity

$$\delta\mathbf{P}^{\alpha}\delta\mathbf{R}^{\beta} = \tfrac{1}{2}([\delta\mathbf{P}^{\alpha}, \delta\mathbf{R}^{\beta}]_{-} + [\delta\mathbf{P}^{\alpha}, \delta\mathbf{R}^{\beta}]_{+}) \quad \text{(A12)}$$

$$= \tfrac{1}{2}\left(\frac{\hbar}{i}\delta_{\alpha\beta} + [\delta\mathbf{P}^{\alpha}, \delta\mathbf{R}^{\beta}]_{+}\right), \quad \text{(A13)}$$

and dropping symmetrized products of second or third order, we find

$$\frac{d}{dt}\delta P^{\alpha}_{jk} \approx \frac{-i}{\hbar}[\hat{V}, \delta\hat{P}^{\alpha}]_{jk} + \frac{1}{2}(\hat{F}^{\alpha}\hat{\sigma} + \hat{\sigma}\hat{F}^{\alpha})_{jk} - \frac{1}{2}\sum_{\beta}(\hat{K}^{\alpha\beta}\delta\hat{R}^{\beta} + \delta\hat{R}^{\beta}\hat{K}^{\alpha\beta})_{jk} - F^{\alpha}_{SH}\sigma_{jk}. \quad \text{(A14)}$$

Equations (A7) and (A14) are the desired results, matching Eqs. (24) and (26). For a more general derivation of these equations, see Ref. 48.

2. Calculation of exact quantum results

For the first three model problems, the exact quantum results in this paper have been computed in MATLAB by time-dependent quantum mechanics using a finite one-dimensional grid and an FFT transformation to represent the momentum operator. Except for the resonance peak in transmission (at $k \approx 29$) in Fig. 6, empirically the branching ratios did not depend sensitively on the width of the incoming wave packet. For problems #1 and #2, the width of the incoming wave packet was chosen as 2 a.u., and for problem #3, the width was 3 a.u. For problem #3, we were unable to quantify exactly how much bigger the transmission peak should be at $k = 29$ a.u. (in the limit of an incoming k-state with infinite spatial width, i.e., a plane wave): our MATLAB calculations became prohibitively expensive.[64] After diagonalizing the total Hamiltonian and propagating the wave packet for a small time Δt, we used a masking function along the boundaries of the grid to eliminate outgoing particle density, while simultaneously measuring the distribution of this flux over the different electronic states. For all cases except the resonant transmission peak in Fig. 6, we estimate that our branching ratios are correct to within 1%. More accurate results are certainly possible (see, e.g., Ref. 65).

For the fourth model problem, where the width of the incoming wave packet was crucial, we computed the exact scattering results for a plane wave ($a_P = 0$ in Fig. 8) using a modified complex Kohn scattering algorithm over a grid in real space, roughly following Ref. 60.

[1] A. M. Wodtke, J. C. Tully, and D. J. Auerbach, Int. Rev. Phys. Chem. **23**, 513 (2004).
[2] M. D. Newton, in *Electron Transfer in Chemistry*, edited by V. Balzani (Wiley-VCH Verlag, New York, 2001), p. 3.
[3] M. Bixon and J. Jortner, Adv. Chem. Phys. **106**, 35 (1999).
[4] R. A. Marcus, J. Phys. Chem. **67**, 853 (1963).
[5] R. A. Marcus and N. Sutin, Biochim. Biophys. Acta **811**, 265 (1985).
[6] P. F. Barbara, T. J. Meyer, and M. A. Ratner, J. Phys. Chem. **100**, 13148 (1996).
[7] S. Jang, Y. Jung, and R. J. Silbey, Chem. Phys. **275**, 319 (2002).
[8] D. Beljonne, C. Curutchet, G. D. Scholes, and R. J. Silbey, J. Phys. Chem. B **113**, 6583 (2009).
[9] A. Nitzan, *Chemical Dyanmics in Condensed Phases* (Oxford University Press, New York, 2006).
[10] G. Schatz and M. A. Ratner, *Quantum Mechanics in Chemistry* (Dover Publications, New York, 2002).
[11] A. D. McLachlan, Mol. Phys. **8**, 39 (1964).
[12] H. D. Meyer and W. H. Miller, J. Chem. Phys. **72**, 2272 (1980).
[13] J. C. Tully, J. Chem. Phys. **93**, 1061 (1990).
[14] J. C. Tully, Faraday Discuss. **110**, 407 (1998).
[15] J. Y. Fang and S. Hammes-Schiffer, J. Phys. Chem. A **103**, 9399 (1999).
[16] R. Kapral and G. Ciccotti, J. Chem. Phys. **110**, 8919 (1999).
[17] S. Nielsen, R. Kapral, and G. Ciccotti, J. Chem. Phys. **112**, 6543 (2000).
[18] R. Grunwald, A. Kelly, and R. Kapral, in *Energy Transfer Dynamics in Biomaterial Systems*, edited by I. Burghardt (Springer-Verlag, Berlin, 2009), p. 383.
[19] I. V. Z. Aleksandrov, Naturforscher. **36a**, 902 (1981).
[20] W. Boucher and J. Traschen, Phys. Rev. D **37**, 3522 (1988).
[21] W. Y. Zhang and R. Balescu, J. Plasma Phys. **40**, 199 (1988).
[22] R. Balescu and W. Y. Zhang, J. Plasma Phys. **40**, 215 (1988).
[23] A. Anderson, Phys. Rev. Lett. **74**, 621 (1995).
[24] O. V. Prezhdo and V. V. Kisil, Phys. Rev. A **56**, 162 (1997).
[25] C. C. Martens and J. Y. Fang, J. Chem. Phys. **106**, 4918 (1997).
[26] A. Donoso and C. C. Martens, J. Phys. Chem. A **102**, 4291 (1998).
[27] D. A. Micha and B. Thorndyke, Int. J. Quant. Chem. **90**, 759 (2002).
[28] H. D. Meyer and W. H. Miller, J. Chem. Phys. **70**, 3214 (1979).
[29] G. Stock and M. Thoss, Phys. Rev. Lett. **78**, 578 (1997).
[30] F. Webster, P. J. Rossy, and R. A. Friesner, Comput. Phys. Comm. **63**, 494 (1991).
[31] F. Webster, E. T. Wang, P. J. Rossy, and R. A. Friesner, J. Chem. Phys. **100**, 4835 (1994).
[32] B. J. Schwartz, E. R. Bittner, O. V. Prezhdo, and P. J. Rossky, J. Chem. Phys. **104**, 5942 (1996).
[33] K. F. Wong and P. J. Rossky, J. Chem. Phys. **116**, 8418 (2002).
[34] K. F. Wong and P. J. Rossky, J. Chem. Phys. **116**, 8429 (2002).
[35] O. V. Prezhdo and P. J. Rossky, J. Chem. Phys. **107**, 825 (1997).
[36] O. V. Prezhdo, J. Chem. Phys. **111**, 8366 (1999).
[37] M. J. Bedard-Hearn, R. E. Larsen, and B. J. Schwartz, J. Chem. Phys. **123**, 234106 (2005).
[38] R. E. Larsen, M. J. Bedard-Hearn, and B. J. Schwartz, J. Phys. Chem. B **110**, 20055 (2006).
[39] Y. L. Volobuev, M. D. Hack, M. S. Topaler, and D. G. Truhlar, J. Chem. Phys. **112**, 9716 (2000).
[40] M. D. Hack and D. G. Truhlar, J. Chem. Phys. **114**, 2894 (2001).
[41] A. W. Jasper, M. D. Hack, and D. G. Truhlar, J. Chem. Phys. **115**, 1804 (2001).
[42] C. Zhu, A. W. Jasper, and D. G. Truhlar, J. Chem. Phys. **120**, 5543 (2004).
[43] C. Zhu, S. Nangia, A. W. Jasper, and D. G. Truhlar, J. Chem. Phys. **121**, 7658 (2004).
[44] A. W. Jasper and D. G. Truhlar, J. Chem. Phys. **123**, 064103 (2005).
[45] J. Y. Fang and S. Hammes-Schiffer, J. Chem. Phys. **110**, 11166 (1999).
[46] E. Neria and A. Nitzan, J. Chem. Phys. **99**, 1109 (1993).
[47] J. R. Schmidt, P. V. Parandekar, and J. C. Tully, J. Chem. Phys. **129**, 044104 (2008).
[48] A. P. Horsfield, D. R. Bowler, A. J. Fisher, T. N. Todorov, and C. G. Sanchez, J. Phys.: Condens. Matter **16**, 8251 (2004).
[49] E. J. Heller, J. Chem. Phys. **75**, 2923 (1981).
[50] A. L. Thompson, C. Punwong, and T. J. Martinez, Chem. Phys. **370**, 70 (2010).
[51] The exact form of the decoherence rate in the Schwartz algorithm is $1/\tau_{\text{Schwartz}}$, $k = |\Sigma_{ij} F_{ij}\sigma_{ji} - F_{kk}|a_X/\hbar$.where the rate now depends on the surface we are collapsing to (here, labeled k). To derive this equation, one must extend the expansion in Eqs. (9) and (10) to second order (Ref. 32).
[52] J. E. Subotnik, J. Chem. Phys. **132**, 134112 (2010).
[53] A. P. Horsfield, D. R. Bowler, A. J. Fisher, T. N. Todorov, and C. G. Sanchez, J. Phys.: Condens. Matter **17**, 4793 (2005).
[54] L. Stella, M. Meister, A. J. Fisher, and A. P. Horsfield, J. Phys.: Condens. Matter **127**, 214104 (2007).
[55] E. J. McEniry, D. R. Bowler, D. Dundas, A. P. Horsfield, C. G. Sanchez, and T. N. Todorov, J. Phys.: Condens. Matter **19**, 196201 (2007).
[56] T. J. Martinez, M. Ben-Nun, and R. D. Levine, J. Phys. Chem. **100**, 7884 (1996).
[57] M. Ben-Nun and T. J. Martinez, J. Chem. Phys. **112**, 6113 (2000).
[58] S. D. Yang, J. D. Coe, B. Kaduk, and T. J. Martinez, J. Chem. Phys. **130**, 134113 (2009).
[59] Note that, as an alternative to FSSH dynamics, the MMST formalism solves this problem correctly without applying collapsing events to force decoher-

ence. In this case, coherent trajectories interfere by phase cancellation, and one finds the correct branching ratios (Refs. 66–68).
[60]J. E. Subotnik and A. Nitzan, J. Chem. Phys. **129**, 144107 (2008).
[61]Note, however, that the expressions for decoherence in this paper and in Ref. 52 are not completely analogous. In particular, the equations of motion in Ref. 52 are only approximate, for they were based on Ehrenfest dynamics rather than the quantum Liouville equation. In this paper, we have the correct equations of motion, and we have shown the approximations necessary to rigorously derive Eq. (55).
[62]E. J. Heller and D. Beck, Chem. Phys. Lett. **202**, 350 (1993).
[63]E. J. Heller, B. Segev, and A. V. Sergeev, J. Phys. Chem. B **106**, 8471 (2002).
[64]Both the FSSH and A-FSSH algorithms predict there should be nearly 100% transmission near $k = 29$ a.u. for an incoming wave packet with infinite spatial width (i.e., a plane wave).
[65]D. Kosloff and R. Kosloff, J. Comp. Phys. **52**, 35 (1983).
[66]X. Sun and W. H. Miller, J. Chem. Phys. **106**, 6346 (1997).
[67]W. H. Miller, J. Chem. Phys. **127**, 084114 (2007).
[68]W. H. Miller, J. Phys. Chem. A **113**, 1405 (2009).